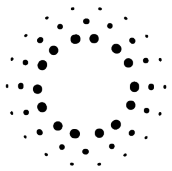

IFT - UNESP
INSTITUTO DE FÍSICA TEÓRICA

MASTER'S THESIS IFT–T.004/2025

Generalized Effective Medium Theory for Elastic Systems with Correlated Disorder

Jorge Mario Escobar Agudelo

Advisor

Danilo Barbosa Liarte

March 2025

Escobar Agudelo, Jorge Mario
E74g Generalized effective medium theory for elastic systems with correlated disorder / Jorge Mario Escobar Agudelo. -- São Paulo, 2025
95 f: il. color.

Dissertação (mestrado) – Universidade Estadual Paulista (Unesp), Instituto de Física Teórica (IFT), São Paulo
Orientador: Danilo Liarte

1. Matéria condensada macia. 2. Transformações de fase (Física estatística). 3. Fenômenos críticos (Física). 4. Correlação (Estatística). 5. Sólidos elásticos. I. Título

Sistema de geração automática de fichas catalográficas da Unesp. Biblioteca do Instituto de Física Teórica (IFT), São Paulo. Dados fornecidos pelo autor(a).

GENERALIZED EFFECTIVE MEDIUM THEORY FOR ELASTIC SYSTEMS WITH CORRELATED DISORDER

Dissertação de Mestrado apresentada ao Instituto de Física Teórica do Câmpus de São Paulo, da Universidade Estadual Paulista "Júlio de Mesquita Filho", como parte dos requisitos para obtenção do título Mestre em Ciências, área: Física.

Comissão Examinadora:

Prof. Dr. DANILO BARBOSA LIARTE (Orientador)
Instituto de Física Teórica/UNESP

Profa. Dra. CAROLINA BRITO CARVALHO DOS SANTOS
Universidade Federal do Rio Grande do Sul/UFRGS

Prof. Dr. ANDRÉ DE PINHO VIEIRA
Instituto de Física da Universidade de São Paulo/IFUSP

Conceito: Aprovado

São Paulo, 04 de abril de 2025.

To my inner child

...

Acknowledgments

First and foremost, I want to take a moment to acknowledge the journey that brought me here. There were many challenges along the way, but I am grateful for persevering and believing in myself, since it has led me to where I am today, and for that, I am deeply thankful. However, as Madonna says, "I can't really make it alone," and that is why I want to use this space to first thank the people who have done the most for me: my parents and my sister, who are always present in everything I do, as well as Tommy, who was with us for many years and is no longer here. My friends and my family in Colombia, especially my chosen sisters Isabella and Melissa, represent a very important part of my life, as does the university I come from, Univalle, for provide valuable tools to begin this journey.

In Brazil, I found great friends and something very close to a family, a place that feels like a home. I thank Angelo and Fefe for being my quirky and insightful place to grow and discover myself. I am grateful to the IFT at UNESP for equipping me with tools to become a professional, but above all, for the incredible people I met, such as the first friends I made and shared a precious LGBTQIA+ bond with, Gabriel and Denise; my outrageous friend and charming neighbor Washington; and, remarkably, my twin sister and partner in crime and *servindo muito*, Juliana. Lastly, to QMLM for always being by my side.

In a very special way, I want to thank my advisor, Dr. Danilo Barbosa Liarte, for being an important guide and support, also an inspirational leader, and for making this process as pleasant as exciting. I also thank Rui Aquino for his valuable collaboration and contribution to the project. This research was made possible thanks to the financial support provided by the São Paulo Research Foundation (FAPESP) under grant number 2023/00067-0.

I am deeply grateful to everyone and to life itself for making all this possible.

"When did we all stop believing in magic?
Why did we put all our hopes in a box in the attic?"

Katy Perry, *Daisies*

Resumo

Este trabalho desenvolve uma generalização da coherent potential approximation (CPA) para estudar transições de rigidez em sistemas elásticos com desordem correlacionada, inspirado nas propriedades mecânicas de géis coloidais macios. Ao estender as teorias de meio efetivo tradicionais, incorporamos correlações espaciais na distribuição de probabilidade da desordem, permitindo a análise de sistemas mais complexos. A estrutura é implementada numericamente utilizando uma rede triangular como caso de teste, aproveitando simetrias e aproximações para simplificar a condição de autocoerência.

Nossa principal contribuição é a formulação de uma ferramenta teórica versátil capaz de descrever transições de rigidez em uma ampla variedade de sistemas desordenados, incluindo aqueles com desordem correlacionada. Como demonstração, aplicamos a estrutura a um modelo inspirado em géis coloidais, revelando que as correlações espaciais deslocam o parâmetro crítico p_c para as transições de rigidez, mas não alteram o número de coordenação z no qual a rigidez ocorre, consistente com o critério de Maxwell ($z_c = 2d$). Além disso, observamos invariância de escala no sistema, indicando comportamento universal próximo à transição crítica. Esses resultados validam a robustez da CPA generalizada e destacam seu potencial para estudar materiais complexos, como redes granulares, tecidos biológicos e metamateriais mecânicos.

Palavras Chaves: Correlated Disorder; Effective Medium Theory; Rigidity Transitions; Soft Colloidal Gels; Elasticity.

Áreas do conhecimento: Condensed Matter; Soft Matter; Phase Transistions and Critical Phenomena
Statistical Mechanics; Complex and Disordered Systems; Effective Medium Theories.

Abstract

This work develops a generalized coherent potential approximation (CPA) framework to study rigidity transitions in elastic systems with correlated disorder, inspired by the mechanical properties of soft colloidal gels. By extending traditional effective medium theories, we incorporate spatial correlations into the probability distribution of disorder, enabling the analysis of more complex systems. The framework is implemented numerically using a triangular lattice as a test case, leveraging symmetries and approximations to simplify the self-consistency constraint.

Our primary contribution is the formulation of a versatile theoretical tool capable of describing rigidity transitions in a wide range of disordered systems, including those with correlated disorder. As a demonstration, we apply the framework to a model inspired by colloidal gels, revealing that spatial correlations shift the critical parameter p_c for rigidity transitions but do not alter the coordination number z at which rigidity occurs, consistent with Maxwell's criterion ($z_c = 2d$). Additionally, we observe scale invariance in the system, indicating universal behavior near the critical transition. These results validate the robustness of the generalized CPA and highlight its potential for studying complex materials such as granular networks, biological tissues, and mechanical metamaterials.

Key Words: Correlated Disorder; Effective Medium Theory; Rigidity Transitions; Soft Colloidal Gels; Elasticity.

Fields of Knowledge: Condensed Matter; Soft Matter; Phase Transistions and Critical Phenomena
Statistical Mechanics; Complex and Disordered Systems; Effective Medium Theories.

Contents

Chapter 1

Introduction

In condensed matter physics, the study of solids has traditionally relied on the crystalline lattice model, providing profound insights into periodic structures [1, 2]. However, many materials in nature exhibit disordered or amorphous arrangements, presenting unique challenges and opportunities for theoretical exploration [3, 4]. Among them, colloidal gels stand out as a fascinating class of soft solids, where attractive interactions between particles form disordered networks with remarkable mechanical and transport properties [5–7]. Understanding their rigidity, particularly in the context of rigidity percolation, remains a central problem in the field.

Rigidity percolation describes the transition from a floppy state—lacking structural rigidity—to a rigid, solid-like state as connectivity increases. Both states can be disordered, but they differ in mechanical stability. This phenomenon is typically associated with Maxwell's isostatic threshold, $z_c = 2d$, for central-force interactions [3, 8, 9]. However, real-world systems like colloidal gels exhibit structural correlations that challenge this classical framework. Recent work shows that such correlations can shift the rigidity transition to lower volume fractions while preserving critical exponents [10], raising the question: can correlations induce rigidity below the isostatic threshold, a state known as subisostaticity?

Motivated by these questions, this work develops a generalized framework for studying disordered systems with spatial correlations. We extend the Coherent Potential Approximation (CPA), a cornerstone of effective medium theory (EMT), to incorporate correlated disorder. Traditional CPA maps disordered networks onto effective homogeneous media using a self-consistency constraint [9, 11, 12], but it does not naturally account for structural correlations. Our generalization introduces a bond-removal protocol that captures these effects by removing blocks of bonds with varying probabilities, broadening the applicability of EMT and providing a powerful tool for studying correlated systems.

To test this framework, we apply it to rigidity percolation in systems like colloidal gels. Our analysis shows that while structural correlations influence rigidity, they do not alter the *critical coordination number* at which it emerges. This highlights the importance of coordinated particle organization rather than a reduction in connectivity. These results, obtained within a specific approximation, will be discussed in detail in later chapters.

This thesis is structured as follows: Part I introduces the foundation for studying rigidity transitions with traditional CPA. Chapter 2 overviews rigidity and its relationship with spatial correlations. Chapter 3 presents classical harmonic crystal theory, which forms the theoretical foundation of EMT. Chapter 4 details the CPA for mapping disordered systems onto homogeneous networks.

Part II generalizes this framework and proposes a simple model based on colloidal gels to apply this method. Chapter 5 introduces a bond-removal process extending CPA to more general systems. Chapter 6 develops a simple model incorporating correlations, supported by numerical corroboration. Chapter 7 presents the conclusions.

This work aims to bridge the gap between uncorrelated and correlated rigidity percolation models by providing a theoretical framework that captures the impact of structural correlations on the rigidity transition. By expanding the tools available for studying these complex systems, we hope to contribute to a deeper understanding of the fundamental principles governing rigidity in disordered materials.

Part I

Effective Medium Theory for Rigidity Transitions

Chapter 2

Rigidity Transitions: A Bird's Eye View

In condensed matter physics, modeling the structure of solids using crystalline lattices has been a cornerstone for understanding their properties and predicting their behavior [1]. This approach has been widely adopted and remains a central framework in the study of matter [2]. However, in nature, a vast number of materials deviate from periodic structures and exhibit disordered arrangements, as illustrated in Figure 2.1. These materials, known as amorphous solids, represent a fascinating and diverse area of study due to their unique features [3, 4].

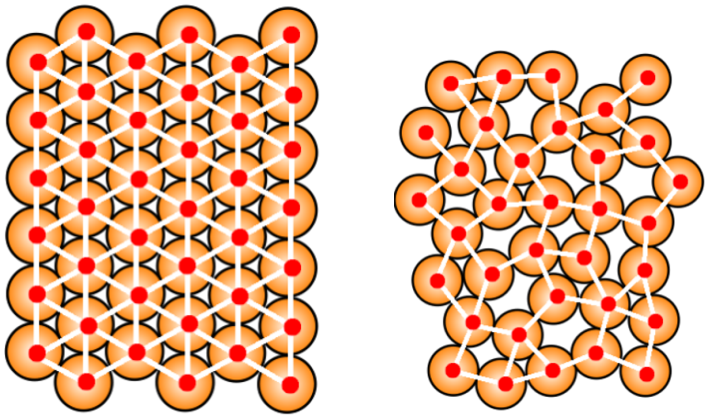

(a) Crystalline solid (b) Amorphous solid

Figure 2.1: Schematic representation of (a) the periodic structure of a crystalline solid and (b) the disordered structure of an amorphous solid.

One of the defining challenges in studying amorphous solids is their incompatibility with traditional crystalline descriptions. As a result, many of the theoretical frameworks and tools developed for periodic systems are not applicable to these disordered materials. To date, no general theory has been developed that comprehensively describes all disordered structures. Consequently, research in this field often focuses on the specific properties of individual systems, presenting both significant challenges and exciting opportunities for exploring open questions in condensed matter physics [9, 13–15].

Effective medium theories (EMTs) of random elastic networks have been commonly employed to model properties like dissipation and rigidity of disordered systems [11, 12, 16–19]. Examples of disordered materials include randomly packed spheres [20–22], granular media [23, 24], proteins [25], polymers [18, 26], network glasses [27–30], and biopolymer gels [31–38]. Among these, a particularly intriguing class is that of colloidal gels, which belong to the category of soft solids [6, 7, 10, 39–41]. These systems are characterized by attractive interactions between colloidal particles suspended in a solvent, usually liquid, where the particles form disordered networks, as shown in Figure 2.2. These networks exhibit unique structural and dynamical properties that make them a rich subject of study in condensed matter physics.

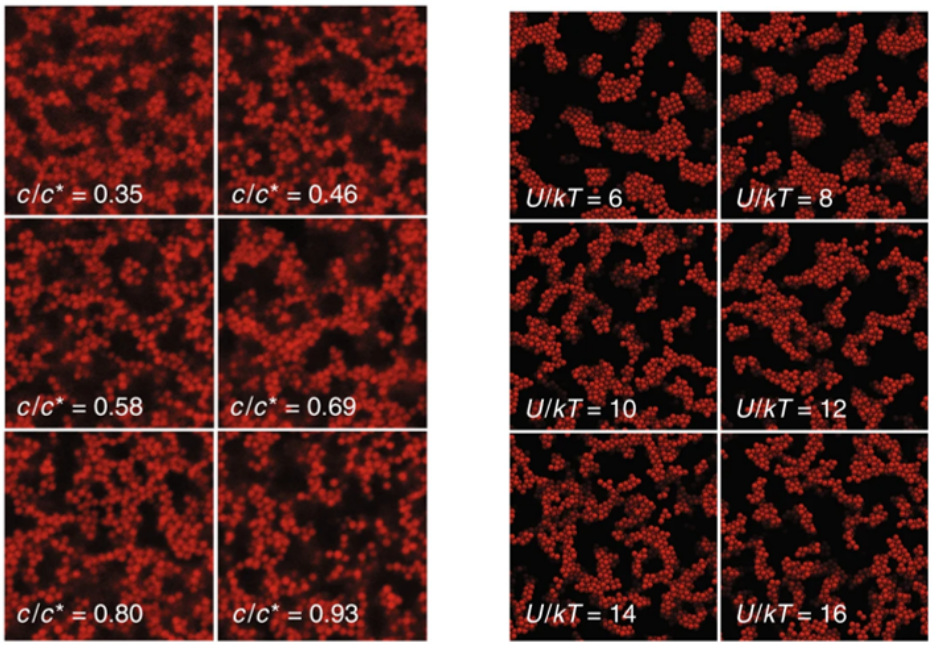

(a) (b)

Figure 2.2: Disordered microstructure of colloidal gels. (a) Confocal micrographs and (b) simulation snapshots of depletion gels at different polymer concentration and fixed volume fraction $\phi = 0.20$. The experimental system employs a model depletion gel designed to simultaneously measure rheology, microstructure, and particle interactions, providing a comprehensive understanding of the gel's microscopic properties and macroscopic elastic response. Simulations use a Brownian dynamics algorithm to generate gel structures and compute their elastic modulus, enabling direct comparison with experimental results. This combined approach aims to elucidate the origins of elasticity in colloidal gels formed by arrested phase separation. Image credit: Adapted from [41].

Due to the attractive interactions that characterize colloidal gels, these systems exhibit a correlated structure that significantly influences their elastic properties [10]. Understanding their rigidity is therefore crucial, yet traditional criteria for analyzing disordered structures often fail to account for the spatial correlations present in such systems. This limitation highlights the need for a more comprehensive theoretical framework capable of describing correlated disorder. In this chapter, we will first introduce the physical and topological principles underlying rigidity percolation, followed by an analysis of the correlated structure of colloidal gels. These discussions provide the necessary foundation for addressing the broader challenge of understanding the properties of systems with correlated disorder, a challenge that will be tackled in subsequent chapters through the development of a generalized EMT.

2.1 Mechanical stability

The solid state of matter is characterized by its ability to resist macroscopic deformations, a property commonly referred to as rigidity. The continuous transition from fluidity to rigidity in disordered solids at zero temperature has been extensively studied based on the assumption that the structure of the material can be described using networks. These networks, in their simplest form, consist of nodes connected by central-force (CF) elastic bonds. This framework thus allows for the study of their spatial distribution and configurations, providing criteria to determine when the system exhibits rigidity [14, 19].

In contrast to crystalline solids, where the periodic arrangement of atoms can be fully described by a set of lattice vectors, disordered systems lack such regularity. The vast variety of possible arrangements in a disordered network makes a purely geometric characterization infeasible, as there is no unique or simple way to describe the spatial distribution of nodes and bonds. This complexity necessitates alternative approaches that focus on global properties rather than local geometric details. One such approach, grounded in topology, shifts the focus from the specific spatial arrangement of particles to the broader connectivity and constraints within the network. By analyzing the balance between degrees of freedom and constraints, these counting methods provide a powerful framework for understanding the mechanical stability of disordered systems [14]. In the following subsection, we will explore Maxwell's criterion for rigidity [8].

2.1.1 Maxwell's criterion for rigidity

The key idea behind Maxwell's criterion involves considering global properties of a network, where rigidity depends on the balance between the system's degrees of freedom and the constraints imposed by the bonds. Rigidity occurs when the number of constraints is at least equal to the number of degrees of freedom, while the existence of spatially unconstrained soft modes leads to a loss of rigidity. This approach, known as soft mode counting, provides a widely recognized method for determining the rigidity of systems that can be represented as networks [8].

Maxwell's criterion establishes the minimum number of constraints required to eliminate soft modes. Consider a d-dimensional lattice of N points connected by CF elastic bonds. The number of degrees of freedom is dN. In the absence of any bonds, the number of soft modes equals the number of degrees of freedom. When constraints are introduced, the number of soft modes, N_0, is given by:

$$N_0 = dN - N_c, \tag{2.1}$$

where N_c represents the total number of constraints imposed by the bonds, which restrict the distance between linked particles. This equation reflects the balance between degrees of freedom and constraints. Each bond, shared between two points, contributes $\frac{1}{2}z$ to the total number of constraints, where z is the coordination number, i.e., the average number of neighbors per site in the network. Assuming that every bond provides an independent constraint, the number of soft modes can be expressed as:

$$N_0 = dN - \frac{1}{2}zN. \tag{2.2}$$

The critical coordination number below which soft modes exist is then given by $z_c = 2d$. When $z \geq z_c$, the system becomes rigid. The specific condition where the number of constraints equals the degrees of freedom, corresponding to $z = z_c$, is known as the isostatic state. This state represents a critical point for rigidity in the system [8, 42, 43].

Maxwell's criterion states then that systems with CF interactions acting as springs between pairs of nodes only become rigid above the isostatic connectivity threshold [3, 4, 8, 9, 12, 44]. However, caution is required when applying this counting argument, as it may lead to overcounting of constraints. This occurs

when bonds are added in regions of the network where no soft modes remain, resulting in states of self-stress that do not contribute to rigidity. To address this issue, it is possible to generalize constraint counting arguments to incorporate the effects of states of self-stress [14, 16, 45].

By adopting a topological description and disregarding geometric details, disordered structures can be represented by randomly assigning constraints within the network [14]. These constraints allow the structure of amorphous solids to be described as random elastic networks where connectivity effects near the isostatic point can be studied by adding or removing bonds according to a probability distribution [9]. These ideas were first introduced in the context of glasses by Phillips [46] and Thorpe [3], who applied Maxwell's criterion to understand the rigidity of amorphous solids. Later, Guyon et al. [47] extended this framework to granular packings, demonstrating its versatility in describing disordered systems.

While Maxwell's criterion provides a fundamental framework for understanding rigidity in networks, it is particularly insightful when applied to the study of phase transitions in disordered systems. Two key concepts in this context are rigidity percolation and jamming, both of which describe the emergence of rigidity as the connectivity or density of a system increases. In the following section, we will explore these phenomena, their interplay, and their significance for understanding the mechanical stability of amorphous solids.

2.1.2 Rigidity percolation and jamming

At the onset of solidity, rigidity percolation is a phase transition, observed in the thermodynamic limit, where the probability of finding a rigid cluster that spans the entire system changes from 0 to 1 [14]. This implies that random elastic networks become increasingly rigid as z grows, exhibiting a CF rigidity percolation transition from floppy clusters to a percolating rigid cluster with a finite elastic modulus at the threshold $z = z_{CF}$, which is near Maxwell's isostatic limit: $z = 2d$ [8, 16, 42, 48].

An alternative approach to studying rigidity in random systems near isostaticity involves the concept of jamming, which describes the behavior of zero-temperature packings of particles. In this framework, the transition from a fluid-

like to a solid-like state occurs as the particle density increases. Specifically, the system evolves from an unjammed disordered state, where particles lack stable contacts, to a jammed disordered state, where particles form a rigid network [22, 49–52]. For frictionless spheres, the coordination number at the jamming transition matches the isostatic critical value $z_c = 2d$ [53–55]. This transition is driven by increasing the volume fraction, ϕ, beyond a critical value, ϕ_c. The isostatic state is continuously approached as the deviation $\Delta\phi = \phi - \phi_c$ approaches zero [12]. A direct relationship exists between particle density, represented by the volume fraction, and the coordination number, given by:

$$\Delta z = z - z_c \sim (\Delta\phi)^{\frac{1}{2}} . \tag{2.3}$$

These parameters are critical for characterizing swollen networks and are associated with elastic moduli. For instance, the shear modulus scales as $G \sim \Delta z$ [12], and the Young's modulus in the case of Poisson ratio of 0.5 is given by $E = 3G$ [6].

Both jamming and rigidity percolation provide suitable frameworks for studying disordered viscoelastic materials near the onset of rigidity [56]. While rigidity percolation focuses on bond connectivity in a network, jamming describes rigidity emergence in densely packed particle systems. These phenomena are deeply connected, as evidenced by their universal scaling forms near the transition point, often studied using EMT [57, 58]. However, Eq. (2.1) primarily applies to systems where CF interactions are the sole contributors to rigidity. In networks with additional interactions, such as bending forces, the system can stabilize below the isostatic limit, a state known as subisostaticity [9, 44, 59]. The role of structural correlations alone in subisostatic stabilization remains uncertain.

Colloidal gels provide a compelling motivation to extend traditional frameworks, as they exhibit additional interactions manifested as correlations among their disordered structural elements [10]. Specifically, incorporating these interactions into a generalized EMT is essential for accurately describing the mechanical properties of these materials. This approach enables an investigation into how structural correlations influence rigidity percolation in colloidal gels, particularly whether they contribute to the emergence of subisostaticity. To achieve this, it is first necessary to characterize the structural correlations present in such systems, which will be analyzed in the following section.

2.2 Structural correlations in colloidal gels

Standard formulations of rigidity percolation, as described previously, do not account for structural correlations. In these models, bonds are removed randomly and independently from the network until the system loses its rigidity [10]. Although this approach has been successfully applied to describe rigidity transitions in certain systems, such as network glasses [29], it is now well-established that the nature of the rigidity transition depends critically on the specific manner in which the final structure is assembled [30, 60, 61]. This observation highlights unresolved fundamental questions regarding the emergence of rigidity in disordered systems. Moreover, theoretical modeling of such transitions becomes particularly challenging in systems exhibiting internal stresses [10]. For example, the presence of attractive interactions has been shown to significantly alter the nature of the rigidity transition in jamming systems [62].

Colloidal aggregates can undergo gelation and form an elastic solid even at arbitrarily low volume fractions, as internal elasticity plays a crucial role in cluster formation [63]. However, the gelation process remains complex and not yet fully understood. The attractive mechanisms responsible for bond formation include van der Waals forces, surface chemistry, hydrophobic effects, and depletion interactions, among others [64]. In some cases, it has been suggested that attractive interactions can exert an effect similar to that of a confining pressure [65].

Motivated by the study of rigidity percolation in systems with correlated disorder, Zhang and colleagues used a lattice model to demonstrate that such correlations shift the percolation transition to lower volume fractions. Moreover, they showed that as the strength of these correlations increases, the percolation threshold decreases further, while the critical exponents characteristic of classical rigidity percolation remain unchanged [10]. These findings raise the question of whether rigidity could emerge even for coordination numbers below the $2d$ threshold, exhibiting subisostaticity. Given that structural correlations lower the volume fraction at which rigidity percolation occurs, one might expect a corresponding shift in the coordination number threshold as well. This possibility serves as the primary motivation for our investigation, as we aim to determine whether and how these correlations influence the mechanical stability of the system.

The onset of rigidity in such systems requires careful consideration of how stresses are transmitted through the material [16]. In attractive colloidal suspensions, these phenomena have been studied experimentally and theoretically using statistical mechanics approaches such as fractal aggregation models, cluster theories, and density functional theories [66–68]. A simplified illustration of how structural correlations shifts the transition to lower volume fractions in these systems was also proposed by Zhang et al. [10] and it is depicted in Figure 2.3.

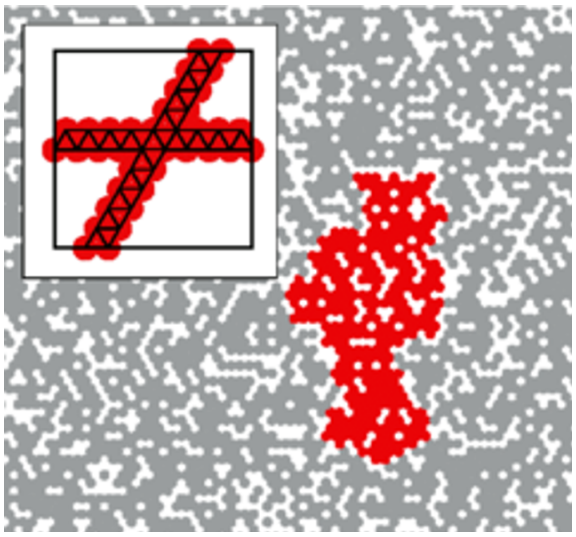

Figure 2.3: Illustration of a rigid cluster decomposition from the correlated lattice model at $\phi_l = 0.6$ with zero correlation strength ($c = 0$). Red particles represent the largest rigid cluster, while gray particles denote the rest of the system. The inset shows a highly correlated configuration where particles assemble into a structure resembling a Warren truss, exhibiting rigidity even at $\phi = 0$ in the thermodynamic limit. This figure is adapted from Zhang et al. (2019) [10].

They explained that correlations drive the assembly of particles into thin, highly organized structures that, in the limit of strong correlations, resemble one-dimensional Warren trusses. These structures are characterized by their ability to efficiently transmit stress along specific directions, effectively reducing the volume fraction required for rigidity in the thermodynamic limit for two-dimensional systems. This explanation highlights the structural role of short-range attractive interactions in guiding the assembly of particles, leading to rigidity at lower volume fractions compared to uncorrelated systems. Consequently, rigidity in colloidal gels is proposed to arise from the coordinated organization of interacting particles, rather than the formation of rigid clusters as suggested in uncorrelated rigidity percolation [10].

Correlated systems thus present new challenges, requiring expanded theoretical approaches to study and understand their unique and complex features. One common tool for analyzing disordered systems is EMT [69–72]. This mean-field theory accounts for disorder by mapping the system onto an effective uniform network, where the parameters are determined using a self-consistency constraint applied to the average disorder, ensuring that replacing a single bond in the effective network results in a local distortion of the strain field that vanishes on average across all possible bond replacements [9, 11, 12, 59]. Motivated by the need to study the elastic properties near the onset of rigidity in systems with spatial correlations, such as colloidal gels, we propose to develop a comprehensive quantitative theory that extends EMT to account for these correlations. This framework will allow us to analyze their influence on the rigidity of gels, particularly focusing on whether the observed shift in volume fraction also leads to a shift in the coordination number, potentially resulting in subisostaticity. With this goal in mind, we now turn to the foundational concepts and mathematical tools that underpin the study of rigidity in elastic networks, which will serve as the basis for our generalized effective medium theory.

Chapter 3

Theory of Classical Harmonic Crystals

To develop a comprehensive understanding of rigidity in disordered systems, such as colloidal gels, we begin by revisiting the Classical Harmonic Crystal Theory, as described by Ashcroft and Mermin [1]. This theory provides useful tools for analyzing the elastic properties of periodic networks, including the dynamical matrix and its relationship with the Green's function, which describe the dynamics of ions around their equilibrium positions at non-zero temperatures. In our context, these ions represent the colloids in a gel. By establishing this theoretical framework, we lay the groundwork for extending our analysis to disordered systems, where structural correlations play a critical role in determining mechanical stability.

To implement this approach, we rely on two assumptions:

1. The mean equilibrium position of each ion is a Bravais lattice site.
2. The typical excursion of each ion from its equilibrium position is small compared to interionic spacing.

Based on these two assumptions, it is possible to propose a harmonic approximation that enables the extraction of quantitative information essential for analyzing our system.

3.1 Harmonic approximation

Due to the first assumption, it is possible to establish a one-to-one correspondence between each ℓ-th ion and the Bravais lattice site located at position $\boldsymbol{R}_\ell$. After the deformation, the position $\boldsymbol{r}_\ell$ of the ion is then a function of $\boldsymbol{R}_\ell$, we then can consider a displacement field on the network that maps particle ℓ initially in $\boldsymbol{R}_\ell$ to a new position $\boldsymbol{r}_\ell(\boldsymbol{R}_\ell)$,

$$\boldsymbol{R}_\ell \longrightarrow \boldsymbol{r}_\ell(\boldsymbol{R}_\ell) = \boldsymbol{R}_\ell + \boldsymbol{u}_\ell(\boldsymbol{R}_\ell), \tag{3.1}$$

which determines $\boldsymbol{u}_\ell$ as the displacement vector (see Figure 3.1).

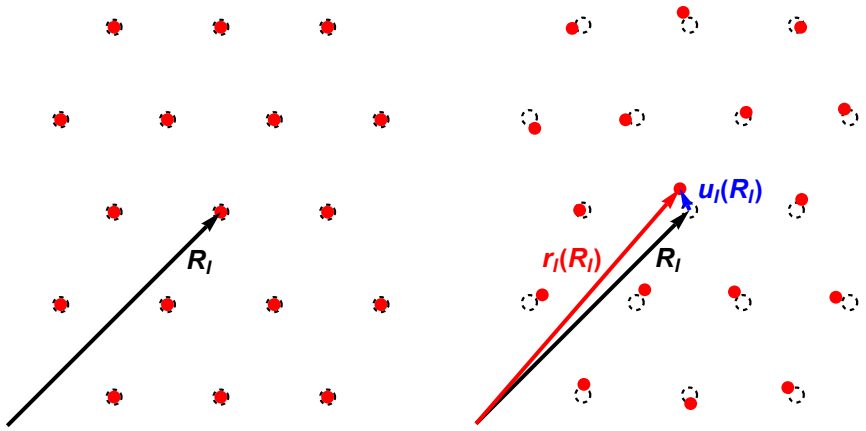

Figure 3.1: (a) Bravais lattice for static models, where the position of each ℓ-th particle is defined by the vector $\boldsymbol{R}_\ell$. (b) Displaced lattice, where the instantaneous position $\boldsymbol{r}_\ell(\boldsymbol{R}_\ell)$ is determined by the equilibrium position $\boldsymbol{R}_\ell$ of each particle and a displacement vector $\boldsymbol{u}_\ell(\boldsymbol{R}_\ell)$, which characterizes the deviation from the equilibrium position.

The interaction potential between pairs can be described in terms of a function ϕ, such that:

$$\begin{aligned} U &= \frac{1}{2}\sum_{\boldsymbol{R},\boldsymbol{R}'} \phi\big(\boldsymbol{r}(\boldsymbol{R}) - \boldsymbol{r}(\boldsymbol{R}')\big) \\ &= \frac{1}{2}\sum_{\boldsymbol{R},\boldsymbol{R}'} \phi\big(\boldsymbol{R} - \boldsymbol{R}' + \boldsymbol{u}(\boldsymbol{R}) - \boldsymbol{u}(\boldsymbol{R}')\big), \end{aligned} \tag{3.2}$$

where $\sum_{\boldsymbol{R}}$ represents the sum over all of the $\boldsymbol{R}_\ell$ vectors in the network. The second assumption implies that all the displacements $\boldsymbol{u}_\ell$ are small, so we can perform a Taylor's expansion in three dimensions:

$$\begin{aligned} U = \underbrace{\phi(\boldsymbol{R} - \boldsymbol{R}')}_{U^{\text{eq}}} + \frac{1}{2}\sum_{\boldsymbol{R},\boldsymbol{R}'} \big[\boldsymbol{u}(\boldsymbol{R}) - \boldsymbol{u}(\boldsymbol{R}')\big] \cdot \underbrace{\nabla\phi\left(\boldsymbol{R} - \boldsymbol{R}'\right)}_{\text{minus force exerted}} \\ \underbrace{+ \frac{1}{4}\sum_{\boldsymbol{R},\boldsymbol{R}'} \big[\big(\boldsymbol{u}(\boldsymbol{R}) - \boldsymbol{u}(\boldsymbol{R}')\big)\cdot\nabla\big]^2\phi\left(\boldsymbol{R} - \boldsymbol{R}'\right)}_{U^{\text{harm}}} + \underbrace{\mathcal{O}(\boldsymbol{u}^3)}_{\to 0}. \end{aligned} \tag{3.3}$$

The linear term vanishes because there is no net force in equilibrium. Additionally, we ignore terms of order higher than two since we assume the displacement is

small. Therefore, the potential energy can be described as the sum of a constant equilibrium term, which can be ignored in dynamical problems, and a harmonic term:

$$U = U^{\text{eq}} + U^{\text{harm}}, \tag{3.4}$$

where the harmonic contribution is given by:

$$\begin{aligned} U^{\text{harm}} &= \frac{1}{4} \sum_{\boldsymbol{R},\boldsymbol{R}'} \left[\left(\boldsymbol{u}_i(\boldsymbol{R}) - \boldsymbol{u}_i(\boldsymbol{R}') \right) \partial_i \right] \cdot \left[\left(\boldsymbol{u}_j(\boldsymbol{R}) - \boldsymbol{u}_j(\boldsymbol{R}') \right) \partial_j \right] \phi \left(\boldsymbol{R} - \boldsymbol{R}' \right) \\ &= \frac{1}{4} \sum_{\boldsymbol{R},\boldsymbol{R}'} \left[\boldsymbol{u}_i(\boldsymbol{R}) - \boldsymbol{u}_i(\boldsymbol{R}') \right] \cdot \frac{\partial^2 \phi \left(\boldsymbol{R} - \boldsymbol{R}' \right)}{\partial r_i \partial r_j} \cdot \left[\boldsymbol{u}_j(\boldsymbol{R}) - \boldsymbol{u}_j(\boldsymbol{R}') \right]. \end{aligned} \tag{3.5}$$

Defining

$$\phi_{ij} \left(\boldsymbol{R} - \boldsymbol{R}' \right) \equiv \frac{\partial^2 \phi \left(\boldsymbol{R} - \boldsymbol{R}' \right)}{\partial r_i \partial r_j}, \tag{3.6}$$

it is possible to write

$$U^{\text{harm}} = \frac{1}{2} \sum_{\boldsymbol{R},\boldsymbol{R}'} \boldsymbol{u}_i(\boldsymbol{R}) \cdot \boldsymbol{D}_{ij}(\boldsymbol{R} - \boldsymbol{R}') \cdot \boldsymbol{u}_j(\boldsymbol{R}'), \tag{3.7}$$

where

$$\boldsymbol{D}_{ij}(\boldsymbol{R} - \boldsymbol{R}') \equiv \delta_{\boldsymbol{R},\boldsymbol{R}'} \sum_{\boldsymbol{R}''} \phi_{ij} \left(\boldsymbol{R} - \boldsymbol{R}'' \right) - \phi_{ij} \left(\boldsymbol{R} - \boldsymbol{R}' \right), \tag{3.8}$$

is the dynamical matrix. This matrix plays a crucial role in characterizing the dynamic behavior of the system. By knowing the type of interaction between particles and the geometry of the lattice, we can construct the matrix and extract essential dynamic information about the system. In the following section we will explore in more detail its construction and fundamental properties.

3.2 Dynamical matrix

In this section, we will treat the dynamical matrix as key operator for extracting dynamic information from the system. Its importance will become evident as we proceed. We will begin by describing the dynamical matrix for a general given

lattice, providing a framework for its construction. To achieve this, we will first introduce its representation in Fourier space, which allows us to express the matrix in terms of the lattice's underlying symmetry and interactions, simplifying the analysis of the system's dynamics.

3.2.1 Fourier transform

Having established the framework for constructing the dynamical matrix, we now turn to its representation in Fourier space. Ignoring the constant equilibrium term, the lattice potential energy can be expressed as a quadratic form:

$$U = \frac{1}{2} \sum_{\ell,\ell'} \boldsymbol{u}_\ell \cdot \boldsymbol{D}_{\ell,\ell'} \cdot \boldsymbol{u}_{\ell'}. \tag{3.9}$$

To facilitate the analysis in Fourier space, we define the Fourier transform of the displacement vectors as:

$$\begin{aligned} \boldsymbol{u}_{\boldsymbol{q}} &= \sum_{\ell} \boldsymbol{u}_\ell \, e^{-i\boldsymbol{q}\cdot\boldsymbol{r}_{\ell 0}}, \\ \boldsymbol{u}_\ell &= \frac{1}{N} \sum_{\boldsymbol{q}} \boldsymbol{u}_{\boldsymbol{q}} \, e^{i\boldsymbol{q}\cdot\boldsymbol{r}_{\ell 0}}. \end{aligned} \tag{3.10}$$

Substituting these Fourier-transformed displacement vectors into the expression for the potential energy, we obtain

$$U = \frac{1}{2N^2} \sum_{\boldsymbol{q},\boldsymbol{q}'} \boldsymbol{u}_{\boldsymbol{q}} \cdot \left(\sum_{\ell,\ell'} \boldsymbol{D}_{\ell,\ell'} \, e^{-i(-\boldsymbol{q})\cdot\boldsymbol{r}_{\ell 0} + i\boldsymbol{q}'\cdot\boldsymbol{r}_{\ell' 0}} \right) \cdot \boldsymbol{u}_{\boldsymbol{q}'}. \tag{3.11}$$

Now, we apply the Fourier transform to the dynamical matrix itself. The Fourier-transformed dynamical matrix is given by:

$$\begin{aligned} \boldsymbol{D}_{\boldsymbol{q},\boldsymbol{q}'} &= \sum_{\ell,\ell'} \boldsymbol{D}_{\ell,\ell'} \, e^{-i\boldsymbol{q}\cdot\boldsymbol{r}_\ell + i\boldsymbol{q}'\cdot\boldsymbol{r}_{\ell'}}, \\ \boldsymbol{D}_{\ell,\ell'} &= \frac{1}{N^2} \sum_{\boldsymbol{q},\boldsymbol{q}'} \boldsymbol{D}_{\boldsymbol{q},\boldsymbol{q}'} \, e^{i\boldsymbol{q}\cdot\boldsymbol{r}_\ell - i\boldsymbol{q}'\cdot\boldsymbol{r}_{\ell'}}. \end{aligned} \tag{3.12}$$

Thus, the potential energy can now be written as:

$$U = \frac{1}{2N^2} \sum_{\boldsymbol{q},\boldsymbol{q}'} \boldsymbol{u}_{\boldsymbol{q}} \cdot \boldsymbol{D}_{-\boldsymbol{q},\boldsymbol{q}'} \cdot \boldsymbol{u}_{\boldsymbol{q}'}. \tag{3.13}$$

At this point, we have successfully expressed the lattice potential energy in Fourier space. This representation is crucial for the subsequent analysis of the system's dynamics, as it highlights the role of the lattice's symmetry and interaction structure. In the following subsection, we will focus on describing this framework for a specific lattice, taking into account the underlying symmetry and the interactions that define the system's behavior.

3.2.2 Description for a lattice

We now proceed to describe the elastic potential energy of a lattice, which consists of a number of bonds b in each of the N unit cells c. To provide a concrete illustration of the general formalism, we first consider the specific case of a triangular lattice, as shown in Figure 3.2.

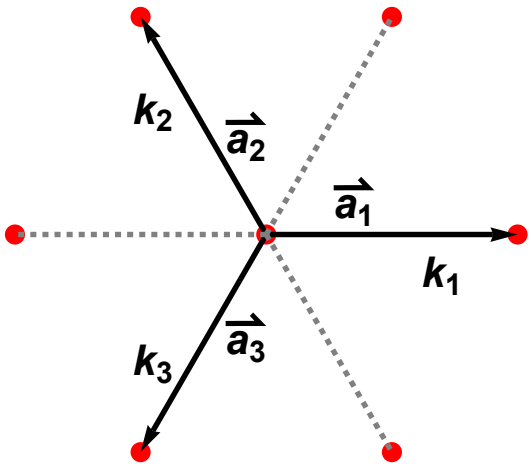

Figure 3.2: Example of the description of a triangular lattice configuration, where the central atom of the unit cell is connected by three of its nearest neighbors by bonds (solid arrows), all the atoms are represented by red dots and the bond is represented by the black arrow (the other lattice connections are shown as dashed lines). Each bond is characterized by a bond strength k_b and a vector $\boldsymbol{a}_b$, which connects the central atom to its neighboring sites. While this arrangement corresponds to a triangular lattice, the general formalism described in the text applies to arbitrary lattice configurations.

In this example, the central atom of the unit cell is connected to its three nearest neighbors by bonds (i.e., $b = 3$), each characterized by a bond strength k_b. The vectors $\boldsymbol{a}_b$ represent the connections between the central atom and its neighboring sites, and their directions are given by the unit vectors $\hat{\boldsymbol{e}}_{\boldsymbol{a}_b}$. This example will serve as a visual and conceptual aid to contextualize the general description that follows.

Returning to the general description, we assume, for simplicity, a uniform bond strength k_b^c across all unit cells. The elastic potential energy of the lattice can then be written as:

$$U = \sum_c \sum_b \frac{k_b^c}{2} \Big[\left(\boldsymbol{u}_{\ell_0^c} - \boldsymbol{u}_{\ell_b^c} \right) \cdot \hat{\boldsymbol{e}}_{\ell_0^c, \ell_b^c} \Big]^2, \tag{3.14}$$

where $\boldsymbol{u}_{\ell_0^c}$ and $\boldsymbol{u}_{\ell_0^c}$ represent the displacements of the two connected atoms by the bond b in the unit cell, and $\hat{\boldsymbol{e}}_{\ell_0^c, \ell_b^c}$ is the unit vector along the bond direction between those two sites. Assuming that the elastic constants k_b^c are organized in the same way across all unit cells, we can drop the unit cell index c and write $k_b^c = k_b$. Here, the index b indicates that the bond strengths may vary within a unit cell, but their spatial arrangement is identical in every unit cell. With this assumption, we next transform the expression for the elastic potential energy into Fourier space:

$$U = \frac{1}{2N^2} \sum_c \sum_b k_b \left[\sum_{\boldsymbol{q}} \boldsymbol{u}_{\boldsymbol{q}} \, e^{i\boldsymbol{q} \cdot \boldsymbol{r}_{\ell_0^c}} \left(1 - e^{i\boldsymbol{q} \cdot \left(\boldsymbol{r}_{\ell_b^c} - \boldsymbol{r}_{\ell_0^c} \right)} \right) \cdot \hat{\boldsymbol{e}}_{\ell_0^c, \ell_b^c} \right]^2. \tag{3.15}$$

We now define $\boldsymbol{a}_b \equiv \boldsymbol{r}_{\ell_b^c} - \boldsymbol{r}_{\ell_0^c}$ as the vector connecting neighboring sites within the unit cell. Note that this definition is specific to the mathematical description used here and should not be confused with the primitive vectors of the lattice, which may differ in certain cases (e.g., in a honeycomb lattice). Since the form of $\boldsymbol{a}_b$ is repeated in each unit cell, we omit the index c. The unit vector $\hat{\boldsymbol{e}}_{\ell_0^c, \ell_b^c}$ can then be rewritten as $\hat{\boldsymbol{e}}_{a_b} = \frac{\boldsymbol{a}_b}{a_b}$, where $a_b = |\boldsymbol{a}_b|$. Substituting this into the expression for U we obtain:

$$U = \frac{1}{2N^2} \sum_{\boldsymbol{q}, \boldsymbol{q}'} \boldsymbol{u}_{\boldsymbol{q}} \cdot \left[\sum_{c,b} k_b e^{i(\boldsymbol{q}+\boldsymbol{q}') \cdot \boldsymbol{r}_{\ell_0^c}} \left(1 - e^{i\boldsymbol{q} \cdot \boldsymbol{a}_b} \right) \left(1 - e^{i\boldsymbol{q}' \cdot \boldsymbol{a}_b} \right) \hat{\boldsymbol{e}}_{a_b} \wedge \hat{\boldsymbol{e}}_{a_b} \right] \cdot \boldsymbol{u}_{\boldsymbol{q}'}, \tag{3.16}$$

where $\hat{\boldsymbol{e}}_{a_b} \wedge \hat{\boldsymbol{e}}_{a_b}$ is the outer product of the unitary vectors. Equation 3.13 allows us to write the dynamical matrix for the lattice:

$$\boldsymbol{D}_{-\boldsymbol{q}, \boldsymbol{q}'} = \sum_{c,b} k_b \, e^{i(\boldsymbol{q}+\boldsymbol{q}') \cdot \boldsymbol{r}_{\ell_0^c}} \left(1 - e^{i\boldsymbol{q} \cdot \boldsymbol{a}_b} \right) \left(1 - e^{i\boldsymbol{q}' \cdot \boldsymbol{a}_b} \right) \hat{\boldsymbol{e}}_{a_b} \wedge \hat{\boldsymbol{e}}_{a_b}. \tag{3.17}$$

We now recognize that this can be expressed in a more compact form as:

$$\begin{aligned} \boldsymbol{D}_{\boldsymbol{q},\boldsymbol{q}'} &= \left(\sum_{c} e^{-i(\boldsymbol{q}-\boldsymbol{q}')\cdot \boldsymbol{r}_{\ell_0^c}} \right) \sum_{b} k_b \left(1 - e^{i\boldsymbol{q}\cdot \boldsymbol{a}_b}\right) \left(1 - e^{i\boldsymbol{q}'\cdot \boldsymbol{a}_b}\right) \hat{\boldsymbol{e}}_{a_b} \wedge \hat{\boldsymbol{e}}_{a_b} \\ &= N\delta_{\boldsymbol{q},\boldsymbol{q}'} \boldsymbol{D}_{\boldsymbol{q}}, \end{aligned} \tag{3.18}$$

with the dynamical matrix in Fourier space defined as:

$$\boldsymbol{D}_{\boldsymbol{q}} \equiv \sum_{b} k_b \left(1 - e^{-i\boldsymbol{q}\cdot \boldsymbol{a}_b}\right) \left(1 - e^{i\boldsymbol{q}'\cdot \boldsymbol{a}_b}\right) \hat{\boldsymbol{e}}_{a_b} \wedge \hat{\boldsymbol{e}}_{a_b}. \tag{3.19}$$

This expression can also be written in terms of a sum over bonds m within the unit cell, leading to the form:

$$\boldsymbol{D}_{\boldsymbol{q}} = \sum_{m} k_m \boldsymbol{B}_{m,\boldsymbol{q}} \wedge \boldsymbol{B}_{m,-\boldsymbol{q}'}, \tag{3.20}$$

where we have defined the B-vector:

$$\boldsymbol{B}_{m,\boldsymbol{q}} \equiv \left(1 - e^{-i\boldsymbol{q}\cdot \boldsymbol{a}_m}\right) \hat{\boldsymbol{e}}_{a_m}. \tag{3.21}$$

This vector is central to the description of the dynamical matrix and, consequently, to the characterization of the lattice's configuration. It encapsulates the structural arrangement of the lattice, specifically encoding the phase relationships and orientations of the bonds, which are crucial for understanding the system's response to perturbations. By leveraging the geometric information contained in the B-vector we can systematically construct the dynamical matrix for the lattice. Here, the index m accounts for each bond within the unit cell.

In the next section, we will use the dynamical matrix derived here to obtain the equations of motion for the lattice. Building on the formalism developed in this chapter, where we have established how to calculate the dynamical matrix for an arbitrary lattice, we will incorporate this expression into the governing equations of the lattice's evolution. This will allow us to formulate the response function, which characterizes the system's behavior under external perturbations and provides insights into its dynamical properties.

3.3 Response Function

One of the most significant properties of the dynamical matrix is its role in solving the differential equation that governs our elastic system. In this section, we will demonstrate how the use of Green's functions enables us to solve this equation effectively. We begin with the equation describing the displacement $\boldsymbol{u}_\ell$ of a lattice point, assuming all points have a mass m; the system is characterized by a damping constant γ, and U represents the elastic potential energy of the system. Additionally, we consider the presence of an external force f_ℓ^{ext} acting on the lattice site ℓ. Thus, the differential equation which describes the dynamics of our system reads as follow:

$$m\ddot{\boldsymbol{u}}_\ell + \gamma\dot{\boldsymbol{u}}_\ell = -\nabla U(\boldsymbol{u}_\ell) + f_\ell^{\text{ext}}. \tag{3.22}$$

First, we compute the gradient using the notation $\nabla U(\boldsymbol{u}_\ell) = \partial U/\partial \boldsymbol{u}_\ell$.

$$\frac{\partial U}{\partial \boldsymbol{u}_\ell} = \sum_q \frac{\partial U}{\partial \boldsymbol{u}_q}\frac{\partial \boldsymbol{u}_q}{\partial \boldsymbol{u}_\ell} = \sum_q \frac{\partial U}{\partial \boldsymbol{u}_q}\frac{\partial}{\partial \boldsymbol{u}_\ell}\left(\sum_{\ell'} \boldsymbol{u}_{\ell'}\, e^{-i\boldsymbol{q}\cdot\boldsymbol{r}_{\ell'}}\right) = \sum_q \frac{\partial U}{\partial \boldsymbol{u}_q}\, e^{-i\boldsymbol{q}\cdot\boldsymbol{r}_\ell}, \tag{3.23}$$

where the Fourier transform in Eq. 3.10 was used. Next, we express the potential energy in terms of the dynamical matrix, as derived in Eq. 3.13,

$$\begin{aligned}\frac{\partial U}{\partial \boldsymbol{u}_\ell} &= \sum_q \frac{\partial}{\partial u_{-q}}\left(\frac{1}{2N^2}\sum_{q',q''} \boldsymbol{u}_{q'}\cdot\boldsymbol{D}_{-q',q''}\cdot\boldsymbol{u}_{q''}\right) e^{i\boldsymbol{q}\cdot\boldsymbol{r}_\ell} \\ &= \frac{1}{N^2}\sum_{q,q'} \boldsymbol{D}_{q,q'}\boldsymbol{u}_{q'}\, e^{i\boldsymbol{q}\cdot\boldsymbol{r}_\ell}.\end{aligned} \tag{3.24}$$

With this information, we calculate the Fourier transform of Eq. (3.22),

$$m\ddot{\boldsymbol{u}}_q + \gamma\dot{\boldsymbol{u}}_q = -\frac{1}{N}\sum_{q'} \boldsymbol{D}_{q,q'}\boldsymbol{u}_{q'} + \tilde{f}_q^{\text{ext}}, \tag{3.25}$$

where $\tilde{f}_q^{\text{ext}}$ is the Fourier transform of the external force. Assuming a solution of the form $\boldsymbol{u}_q(t) = \boldsymbol{u}(q)e^{-i\omega t}$, we apply the method of separation of variables, which allows us to rewrite the linear equation as follows:

$$-\left(m\omega^2 + i\gamma\omega\right)\boldsymbol{u}_q = -\frac{1}{N}\sum_{q'} \boldsymbol{D}_{q,q'}\boldsymbol{u}_{q'} + \tilde{f}_q^{\text{ext}}. \tag{3.26}$$

On the left-hand side of this equation, we have a factor of $\boldsymbol{u}_{\boldsymbol{q}}$, while on the right-hand side, we have a summation over q' and a factor of $\boldsymbol{u}_{\boldsymbol{q}'}$. This structure suggests that the displacement vector in reciprocal space can be modeled using a matrix representation, encapsulating all the information about its possible values included in the summation. This allows us to rewrite the differential equation in a more compact form:

$$-\left[\left(m\omega^2 + i\omega\gamma\right)\mathbb{I} - \frac{1}{N}\boldsymbol{D}\right]\boldsymbol{u} = \tilde{\boldsymbol{f}}^{\text{ext}}. \tag{3.27}$$

where $\boldsymbol{D}$ is an operator acting on all the q' components in the matrix $\boldsymbol{u}$. This shows that Eq. (3.22) takes the form $\boldsymbol{L}(\boldsymbol{q})\boldsymbol{u}(\boldsymbol{q}) = \boldsymbol{f}(\boldsymbol{q})$, where $\boldsymbol{L}$ is a linear differential operator, $\boldsymbol{u}$ represents the solution, and $\boldsymbol{f}$ corresponds to the external source term. Following the theory of Green's functions, it is possible to construct a matrix $\boldsymbol{G}(\boldsymbol{q},\omega)$ in Fourier space, which describes the solution as $\boldsymbol{u}(\boldsymbol{q}) = \int \boldsymbol{G}(\boldsymbol{q},\omega)\boldsymbol{f}(\omega)d\omega$. These functions are widely used to solve differential equations, as they represent the system's response to an external perturbations [73]. In our case, $\boldsymbol{G}(\boldsymbol{q},\omega)$ characterizes the lattice's elastic response to deformations, making it central to our analysis. From Eq. (3.27), we identify the Green's function as:

$$\boldsymbol{G}(\omega) = \left[\left(m\omega^2 + i\omega\gamma\right)\mathbb{I} - \frac{1}{N}\boldsymbol{D}\right]^{-1}, \tag{3.28}$$

This expression highlights a key relationship: the Green's function, $\boldsymbol{G}(\omega)$, depends explicitly on the dynamical matrix $\boldsymbol{D}$. This means that, by constructing the dynamical matrix for our system, we can directly determine its response function, bridging the gap between the lattice's structural properties and its dynamic behavior under external perturbations. In many cases, including ours, it is useful to work with the zero-frequency Green's function, setting $\omega = 0$. For a periodic system with $\boldsymbol{D}_{\boldsymbol{q},\boldsymbol{q}'} = N\delta_{\boldsymbol{q},\boldsymbol{q}'}\boldsymbol{D}_{\boldsymbol{q}}$, the Green's function reduces to:

$$\boldsymbol{G}(0) = -\boldsymbol{D}^{-1}. \tag{3.29}$$

In this section, we have established the response function for our system, linking it to the dynamical matrix. These results provide the foundation for the next chapter, where we will introduce effective medium theory. Building on the classical harmonic crystal framework developed here, we will extend our analysis to systems with disorder and external influences.

Chapter 4

Coherent Potential Approximation

Describing a disordered lattice system with many sites poses significant challenges, making a direct geometric description very difficult [14]. One of the methodologies used to approximate the physical behavior of such systems is effective medium theory [11, 14, 17, 18, 56, 57, 70, 74, 75]. This framework takes advantage of the known macroscopic properties of the system, combined with statistical methods, to average over possible configurations under specific constraints. Among the various formulations of effective medium theory, our approach leverages the derived relationship between the dynamical matrix of the network and the Green's function. This method allows us to implement the coherent potential approximation (CPA) [9, 12, 19, 76].

As a general overview of the model, the objective can be understood as proposing a mapping that enables the description of a disordered network—or equivalently, a diluted network system—through an effective medium characterized by the Green's function of a homogeneous system. For this mapping to be valid, it is necessary to impose a self-consistency constraint on the Green's functions involved. In the following sections, we will provide a detailed description of the traditional CPA, which has been successfully employed in the study of disordered systems [9, 11, 19, 76].

4.1 Formulation of the traditional effective medium

The strategy consists of mapping the disordered system—described as a random, inhomogeneous medium—to a homogeneous, translationally-invariant one with a known and well-defined structure [19]. Starting from the zero-frequency Green's function in Eq. (3.29), and adopting a specific convention for the relationship between $\boldsymbol{D}$ and $\boldsymbol{G}$ that ignores N factors, we assume that the dynamical

matrix $\boldsymbol{D}^V$ of the disordered system can be expressed as:

$$\boldsymbol{D}^V = \boldsymbol{D} + \boldsymbol{V} = -\boldsymbol{G}^{-1} + \boldsymbol{V} = -\left[\boldsymbol{G}^V\right]^{-1}, \tag{4.1}$$

where $\boldsymbol{D}$ represents the dynamical matrix of the homogeneous system, and $\boldsymbol{V}$ is a perturbation matrix that encodes the disorder present in the system. In this context, $\boldsymbol{G}$ and $\boldsymbol{G}^V$ represent the Green's functions of the homogeneous and disordered systems, respectively. Hence, the latter can be expressed as

$$\boldsymbol{G}^V = \left[\boldsymbol{G}^{-1} - \boldsymbol{V}\right]^{-1}. \tag{4.2}$$

We now proceed to expand the Green's function of the disordered system by expressing it as an infinite series, aiming to derive the T-matrix. This central element in the CPA framework captures the effects of disorder in a simplified and effective form, while also enabling us to describe the self-consistency constraint.

4.1.1 Green's function expansion

In order to describe perturbed Green's function, we follow the formalism presented in Elliott and colleagues' review [70], and expand matrices of the form given by Eq. (3.28), where $\boldsymbol{D}_q$ is known—such as in the case of a homogeneous lattice. As derived earlier, the Green's function of a system with defects, $\boldsymbol{G}^V$, can be expressed in terms of the homogeneous and known Green's function, $\boldsymbol{G}$, and a perturbation matrix, $\boldsymbol{V}$. Using Eq. 4.2, the formal solution is given by:

$$\boldsymbol{G}^V = \left[\boldsymbol{G}^{-1} - \boldsymbol{V}\right]^{-1} = \left[\boldsymbol{G}^{-1}(\mathbb{I} - \boldsymbol{G}\boldsymbol{V})\right]^{-1} = (\mathbb{I} - \boldsymbol{G}\boldsymbol{V})^{-1}\boldsymbol{G}. \tag{4.3}$$

This solution admits multiple equivalent representations. A particularly useful one is:

$$\boldsymbol{G}^V = \boldsymbol{G} + \boldsymbol{G}\boldsymbol{T}\boldsymbol{G}, \tag{4.4}$$

where $\boldsymbol{T} = \boldsymbol{V}(\mathbb{I} - \boldsymbol{G}\boldsymbol{V})^{-1}$ is commonly referred to as the T-matrix. Another important representation is the Dyson equation:

$$\boldsymbol{G}^V = \boldsymbol{G} + \boldsymbol{G}\boldsymbol{V}\boldsymbol{G}^V, \tag{4.5}$$

which allows for an infinite expansion:

$$\begin{aligned} \boldsymbol{G}^V &= \boldsymbol{G} + \boldsymbol{GVG} + \boldsymbol{GVGVG} + \boldsymbol{GVGVGVG} + \cdots \\ &= \boldsymbol{G} + \boldsymbol{G}\Big(\boldsymbol{V} + \boldsymbol{VGV} + \boldsymbol{VGVGV} + \cdots\Big)\boldsymbol{G}. \end{aligned} \tag{4.6}$$

From Eq. (4.4), we can derive a general expression for the T-matrix as an infinite series:

$$\boldsymbol{T} = \boldsymbol{V} + \boldsymbol{VGV} + \boldsymbol{VGVGV} + \cdots . \tag{4.7}$$

For a specific system, we can now describe the forms of $\boldsymbol{G}$ and $\boldsymbol{V}$. One of the key contributions of the CPA is the ability to represent this infinite series as a single effective term. In the following section, we will apply the CPA to a random lattice and derive the T-matrix as a geometric series, highlighting this important result.

4.2 Application to a random lattice

The coherent potential approximation (CPA) provides a powerful framework to describe disordered systems, such as random lattices with defects or impurities. Physically, this approach captures the average effect of disorder by replacing the system with an effective medium, whose properties are determined self-consistently. In the context of random lattices, this means encoding the influence of defects into an effective dynamical matrix. The key assumption is that the average response of the disordered system can be well approximated by this effective medium, provided that the self-consistency conditions are satisfied. In the following, we apply this method to derive the effective properties of a random lattice, connecting the physical intuition behind the CPA to its mathematical formulation.

Now that we have provided a general overview of how to describe the Green's function for disordered systems, we can proceed with a more detailed analysis of the method and its underlying assumptions. A disordered system—modeled as a random lattice with defects, described by Green's function $\boldsymbol{G}^V$ and dynamical matrix $\boldsymbol{D}^V$—is mapped onto a homogeneous effective medium, characterized by

its Green's function $\boldsymbol{G}$ and dynamical matrix $\boldsymbol{D}$,

$$\begin{aligned} \boldsymbol{D} \longrightarrow \boldsymbol{D}^V &= \boldsymbol{D} + \boldsymbol{V} \\ \boldsymbol{D}^V_{q,q'} &= \boldsymbol{D}_{q,q'} + \boldsymbol{V}_{q,q'} \\ \boldsymbol{D}^V_{q,q'} &= N\delta_{q,q'}\boldsymbol{D}_q + \boldsymbol{V}_{q,q'}. \end{aligned} \tag{4.8}$$

As discussed earlier, $\boldsymbol{V}$ encodes the scattering information due to the defects. Each of these terms is a matrix dependent on two variables, q and q'.The Green's function of the disordered system can be written as a two-variable function. Using the result from Eq. 3.28, we have:

$$\begin{aligned} \boldsymbol{G}^V &= \left[\Big(m\omega^2 + i\omega\gamma\Big)\mathbb{I} - \frac{1}{N}\boldsymbol{D}^V\right]^{-1} \\ &= \left[\Big(m\omega^2 + i\omega\gamma\Big)\mathbb{I} - \frac{1}{N}\boldsymbol{D} - \frac{1}{N}\boldsymbol{V}\right]^{-1} \\ &= \left[\boldsymbol{G}^{-1} - \frac{1}{N}\boldsymbol{V}\right]^{-1} \\ &= \left\{\boldsymbol{G}^{-1}\left[\mathbb{I} - \frac{1}{N}\boldsymbol{G}\boldsymbol{V}\right]\right\}^{-1} \\ &= \left[\mathbb{I} - \frac{1}{N}\boldsymbol{G}\boldsymbol{V}\right]^{-1}\boldsymbol{G} \\ &= \left[\mathbb{I} + \frac{1}{N}\boldsymbol{G}\boldsymbol{V} + \frac{1}{N^2}\boldsymbol{G}\boldsymbol{V}\boldsymbol{G}\boldsymbol{V} + \frac{1}{N^3}\boldsymbol{G}\boldsymbol{V}\boldsymbol{G}\boldsymbol{V}\boldsymbol{G}\boldsymbol{V} + \cdots\right]\boldsymbol{G} \\ &= \boldsymbol{G} + \frac{1}{N}\boldsymbol{G}\boldsymbol{V}\boldsymbol{G} + \frac{1}{N^2}\boldsymbol{G}\boldsymbol{V}\boldsymbol{G}\boldsymbol{V}\boldsymbol{G} + \frac{1}{N^3}\boldsymbol{G}\boldsymbol{V}\boldsymbol{G}\boldsymbol{V}\boldsymbol{G}\boldsymbol{V}\boldsymbol{G} + \cdots. \end{aligned} \tag{4.9}$$

Referring to the results in Eq. (4.4), we identify the T-matrix as:

$$N\boldsymbol{T}_{q,q'} = \boldsymbol{V}_{q,q'} + \frac{1}{N}\sum_{q_1}\boldsymbol{V}_{q,q_1}\boldsymbol{G}_{q_1}\boldsymbol{V}_{q_1,q'} + \frac{1}{N^2}\sum_{q_1,q_2}\boldsymbol{V}_{q,q_1}\boldsymbol{G}_{q_1}\boldsymbol{V}_{q_1,q_2}\boldsymbol{G}_{q_2}\boldsymbol{V}_{q_2,q'} + \cdots, \tag{4.10}$$

which consists of infinitely many terms. The usual CPA introduces a powerful strategy to address this issue, enabling us to derive an analytical expression for the T-matrix with a single term.

4.2.1 Evaluation of the T-matrix as a geometric series

Having established an expression for the T-matrix in terms of the homogeneous Green's function, we now derive the perturbation matrix $\boldsymbol{V}$, which encodes the effects of defects in the system. To do this, we consider the effective medium as a homogeneous lattice where all bonds are occupied and characterized by an unknown effective spring constant k. In this scenario, the Green's function of the effective medium coincides with that of a homogeneous system.

To model a defect, we replace a single arbitrary bond in the effective medium with a new bond characterized by a spring constant k'. This constant can take two values, for instance:

- $k' = 1$ with a probability p (representing an occupied bond), or
- $k' = 0$ with a probability $1 - p$ (representing an unoccupied bond).

The perturbation matrix $\boldsymbol{V}$ captures the difference between the defective and homogeneous systems. Specifically, it accounts for the replacement of the original bond (with elastic constant k) by the new bond (with spring constant k'). Following the matrix construction developed in Eq. (3.20), the perturbation matrix is given by:

$$\boldsymbol{V}_{q,q'}(k,k') = (k'-k)\boldsymbol{B}_{1,q} \wedge \boldsymbol{B}_{1,-q'} \ , \tag{4.11}$$

where the index "1" refers to the specific bond being replaced. The term $(k'-k)$ ensures that the contribution of the bond in the homogeneous lattice is replaced by a defect [76].

By substituting the expression for the perturbation matrix $\boldsymbol{V}$ into Eq. (4.10), we

can explicitly compute the T-matrix. Replacing $\boldsymbol{V}$ in the series expansion yields:

$$\begin{aligned} N\boldsymbol{T}_{q,q'} &= \boldsymbol{V}_{q,q'} + \frac{1}{N}\sum_{q_1}(k'-k)^2\Big(\boldsymbol{B}_{1,q}\wedge\boldsymbol{B}_{1,-q_1}\Big)\cdot\boldsymbol{G}_{q_1}\cdot\Big(\boldsymbol{B}_{1,q_1}\wedge\boldsymbol{B}_{1,-q'}\Big) \\ &\quad + \frac{1}{N^2}\sum_{q_1,q_2}(k'-k)^3\Big(\boldsymbol{B}_{1,q}\wedge\boldsymbol{B}_{1,-q_1}\Big)\cdot\boldsymbol{G}_{q_1}\cdot\Big(\boldsymbol{B}_{1,q_1}\wedge\boldsymbol{B}_{1,-q_2}\Big) \\ &\qquad\qquad \cdot\boldsymbol{G}_{q_2}\cdot\Big(\boldsymbol{B}_{1,q_2}\wedge\boldsymbol{B}_{1,-q'}\Big)+\cdots \\ &= \boldsymbol{V}_{q,q'} + (k'-k)^2\boldsymbol{B}_{1,q}\wedge\boldsymbol{B}_{1,-q'}\left[\frac{1}{N}\sum_{q_1}\boldsymbol{B}_{1,-q_1}\cdot\boldsymbol{G}_{q_1}\cdot\boldsymbol{B}_{1,q_1}\right] \\ &\quad + (k'-k)^3\boldsymbol{B}_{1,q}\wedge\boldsymbol{B}_{1,-q'}\left[\frac{1}{N}\sum_{q_1}\boldsymbol{B}_{1,-q_1}\cdot\boldsymbol{G}_{q_1}\cdot\boldsymbol{B}_{1,q_1}\right] \\ &\qquad\qquad \left[\frac{1}{N}\sum_{q_2}\boldsymbol{B}_{1,-q_2}\cdot\boldsymbol{G}_{q_2}\cdot\boldsymbol{B}_{1,q_2}\right]+\cdots. \end{aligned} \tag{4.12}$$

Defining the function

$$f(k,\omega) \equiv -\frac{1}{N}\sum_{q}\boldsymbol{B}_{1,-q}\cdot\boldsymbol{G}_{q}\cdot\boldsymbol{B}_{1,q}\,, \tag{4.13}$$

we can express the T-matrix as:

$$\begin{aligned} N\boldsymbol{T}_{q,q'} &= \boldsymbol{V}_{q,q'} - (k'-k)f(k,\omega)\Big[(k'-k)\boldsymbol{B}_{1,q}\wedge\boldsymbol{B}_{1,-q'}\Big] \\ &\quad + (k'-k)^2f^2(k,\omega)\Big[(k'-k)\boldsymbol{B}_{1,q}\wedge\boldsymbol{B}_{1,-q'}\Big]+\cdots \\ &= \boldsymbol{V}_{q,q'} - (k'-k)f(k,\omega)\boldsymbol{V}_{q,q'} + (k'-k)^2f^2(k,\omega)\boldsymbol{V}_{q,q'}+\cdots. \end{aligned} \tag{4.14}$$

We can identify the form of a geometric series,

$$\sum_{k=1}^{\infty} ar^k = \frac{a}{1-r}. \tag{4.15}$$

Therefore,

$$N\boldsymbol{T}_{q,q'} = \frac{\boldsymbol{V}_{q,q'}}{1+(k'-k)f(k,\omega)}. \tag{4.16}$$

This result is powerful, as it provides a straightforward analytical expression for the T-matrix while relying solely on known quantities. Since the structure of the homogeneous network is known, we can construct both the Green's function $\boldsymbol{G}_q$

and the vectors $\boldsymbol{B}_{1,q}$ of the system, making $f(k,\omega)$ and $\boldsymbol{V}_{q,q'}$ well-defined. Using this information, we will now apply the self-consistency constraint of the CPA to compute the effective spring constant k. This will allow us to describe the disordered network through the mapping provided by effective medium theory. For future calculations, we can establish that, in the continuous limit, the function $f(k,\omega)$ can be expressed as [76]:

$$f(k,\omega) = -v_0 \int_{1\text{BZ}} \frac{d^2\boldsymbol{q}}{4\pi^2} \boldsymbol{B}_{1,-q} \cdot \boldsymbol{G}_q \cdot \boldsymbol{B}_{1,q} \tag{4.17}$$

where v_0 is the volume of the unit cell and 1BZ stands for the first Brillouin zone.

4.2.2 Self-consistency constraint

To ensure that the proposed mapping accurately describes the disordered lattice, it is necessary to impose a self-consistency constraint. This condition requires that the Green's function of the homogeneous effective medium matches the average of the perturbed Green's function over the impurity's probability distribution. Mathematically, this can be expressed as:

$$\left\langle \boldsymbol{G}^V \right\rangle_{\text{impurities}} = \boldsymbol{G}. \tag{4.18}$$

Using Eq. (4.4) to compute this average, it follows that the self-consistency constraint implies:

$$\langle \boldsymbol{T} \rangle_{\text{impurities}} = 0, \tag{4.19}$$

indicating that the T-matrix vanishes when averaged over configurations that include the impurity. Subsequently, leveraging our understanding of the T-matrix, we can compute this mean value for the specific probability distribution proposed earlier:

$$k' = \begin{cases} 1, & \text{with probability } p, \\ 0, & \text{with probability } 1-p. \end{cases} \tag{4.20}$$

Thus, we express:

$$\left\langle \boldsymbol{T}_{q,q'} \right\rangle_{\text{impurities}} = p\boldsymbol{T}_{q,q'}\big|_{k'=1} + (1-p)\boldsymbol{T}_{q,q'}\big|_{k'=0} = 0. \tag{4.21}$$

By applying the result from Eq. (4.16), we obtain

$$\begin{aligned} p\,\frac{(1-k)\boldsymbol{B}_{1,\boldsymbol{q}} \wedge \boldsymbol{B}_{1,-\boldsymbol{q}'}}{1+(1-k)f(k,\omega)} + (1-p)\frac{-k\boldsymbol{B}_{1,\boldsymbol{q}} \wedge \boldsymbol{B}_{1,-\boldsymbol{q}'}}{1-kf(k,\omega)} &= 0 \\ f(k,\omega)k^2 - \big[1+f(k,\omega)\big]k + p &= 0. \end{aligned} \tag{4.22}$$

This results in an expression that determines the effective medium spring constant k for any given probability p and frequency ω, successfully describing the disordered network through the proposed mapping [76]. This approach has proven highly effective in modeling diluted systems, as demonstrated by numerous studies [9, 11, 12, 14, 17–19, 52, 74–76]. Building on this framework, our next objective is to generalize the effective medium theory to incorporate correlations present in systems such as colloidal gels. This extension will allow us to evaluate how these correlations influence rigidity percolation and determine whether subisostatic behavior emerges.

In Part I, we introduced the stability criteria that motivate the study of rigidity in disordered structures, emphasizing the importance of incorporating spatial correlations into these descriptions. Traditional effective medium theory does not account for such effects, limiting its applicability to systems like colloidal gels. To address this, we outlined the foundations and key features of this theoretical framework. In Part II, we will focus on our main contribution: a generalization of effective medium theory that incorporates spatial correlations. Inspired by the structural properties of colloidal gels, we will apply this generalized framework to analyze their rigidity and provide new insights into their mechanical behavior.

Part II

Correlated Coherent Potential Approximation

Chapter 5

Generalized Effective Medium Theory

The main goal of this work is to extend the effective medium theory introduced in Chapter 4, which provides a framework for studying disordered networks and their mechanical properties, such as rigidity. This extension focuses on incorporating spatial correlations between elements associated with disorder, enabling a more accurate description and modeling of systems with correlated disorder, such as colloidal gels. The conventional Coherent Potential Approximation (CPA) does not account for these correlations, limiting its applicability to uncorrelated systems. Therefore, our goal is to generalize the effective medium theory to include correlated behaviors and provide a broader framework for analyzing these complex systems.

This generalization requires redefining how bonds are diluted in the network. We propose a framework in which multiple links can be removed simultaneously, with each removed link being associated with a different elastic constant k_i'. This approach generates a more general probability distribution, allowing us to describe a broader range of disordered configurations. In this chapter, we will derive the corresponding T-matrix for this generalized framework and apply the self-consistency constraint to calculate the mean value over all possible defects, extending the usual CPA to this more complex scenario. This step establishes the foundation for analyzing systems with correlated disorder.

To account for spatial correlations between the elements associated with disorder, we will develop a protocol in Chapter 6 that incorporates these correlations into the probability distribution. This protocol plays a key role in refining the theory and enabling the description of correlated disordered systems, such as colloidal gels. The current chapter focuses on building the generalized framework of the effective medium theory, which will serve as the basis for introducing correlations in the subsequent chapter.

5.1 Multiple bond removal with varying probabilities

In the usual CPA, the T-matrix is constructed to account for a single defect in the network. The construction of the perturbation matrix (V-matrix) in Eq. (4.11) is based on this one-bond removal process. To extend the framework to systems with multiple defects, we redefine the V-matrix to describe the simultaneous removal of several bonds. Each bond in this set can have a different elastic constant k_i' and a corresponding probability of being removed, resulting in a more general probability distribution. Thus, the V-matrix can be constructed as the sum of contributions from multiple bonds. Instead of accounting solely for the B-vector of a single bond (e.g., bond "1"), we extend the sum to a set of $i = 1, 2, \ldots, n$ bonds. Mathematically, this can be expressed as:

$$\boldsymbol{V}_{q,q'} = \sum_{i=1}^{n} (k_i' - k) \boldsymbol{B}_{i,q} \wedge \boldsymbol{B}_{i,-q'} \,. \tag{5.1}$$

Here, k represents the elastic constant of the homogeneous network, while each k_i' is determined by a probability distribution that specifies the likelihood of bond removal for the i-th bond in the block.

This new formulation changes the functional form of the T-matrix, which previously enabled us to describe it as a geometric series. In this generalized framework, we cannot assume such a simplification. One of our main challenges now is to find an alternative representation of the infinite sum in a more manageable form, ideally as a single term. We begin with the general expression for the T-matrix given in Eq. (4.10). Here, we use a continuous wave vector to simplify future calculations:

$$\begin{aligned} \boldsymbol{T}_{q,q'} = \boldsymbol{V}_{q,q'} &+ \int_{q_1} d\mathbf{q}_1 \boldsymbol{V}_{q,q_1} \cdot \boldsymbol{G}_{q_1} \cdot \boldsymbol{V}_{q_1,q'} \\ &+ \int_{q_1} \int_{q_2} d\mathbf{q}_1 d\mathbf{q}_2 \boldsymbol{V}_{q,q_1} \cdot \boldsymbol{G}_{q_1} \cdot \boldsymbol{V}_{q_1,q_2} \cdot \boldsymbol{G}_{q_2} \cdot \boldsymbol{V}_{q_2,q'} + \cdots \,, \end{aligned} \tag{5.2}$$

where $\int_q d\mathbf{q}$ represents $v_0 \int_{1\mathrm{BZ}} d^2\boldsymbol{q}/4\pi^2$, with v_0 denoting the unit cell volume, and the integrals are evaluated within the first Brillouin zone, denoted as 1BZ.

Substituting Eq. (5.1) into the above expression, we rewrite the T-matrix as follows:

$$\begin{aligned}\boldsymbol{T}_{q,q'} &= \sum_{i=1}^{n}\left(\frac{k_i'}{k}-1\right)k\boldsymbol{B}_{i,q}\wedge\boldsymbol{B}_{i,-q'}\\ &+\sum_{i,j=1}^{n}\left(\frac{k_i'}{k}-1\right)\left(\frac{k_j'}{k}-1\right)k\boldsymbol{B}_{i,q}\wedge\boldsymbol{B}_{j,-q'}\left(k\int_{q_1}d\mathbf{q}_1\,\boldsymbol{B}_{i,-q_1}\cdot\boldsymbol{G}_{q_1}\cdot\boldsymbol{B}_{j,q_1}\right)\\ &+\sum_{i,j,l=1}^{n}\left(\frac{k_i'}{k}-1\right)\left(\frac{k_j'}{k}-1\right)\left(\frac{k_l'}{k}-1\right)k\boldsymbol{B}_{i,q}\wedge\boldsymbol{B}_{j,-q'}\\ &\times\left(k\int_{q_1}d\mathbf{q}_1\,\boldsymbol{B}_{i,-q_1}\cdot\boldsymbol{G}_{q_1}\cdot\boldsymbol{B}_{l,q_1}\right)\left(k\int_{q_2}d\mathbf{q}_2\,\boldsymbol{B}_{l,-q_2}\cdot\boldsymbol{G}_{q_2}\cdot\boldsymbol{B}_{j,q_2}\right)+\cdots.\end{aligned}\tag{5.3}$$

To simplify this expression, we define the H-matrix, whose (i,j)-th component is given by:

$$H_{ij}\equiv -k\int_{q}d\mathbf{q}\;\boldsymbol{B}_{i,-q}\cdot\boldsymbol{G}_{q}\cdot\boldsymbol{B}_{j,q}.\tag{5.4}$$

This allows us to rewrite the T-matrix in a more compact form:

$$\begin{aligned}\boldsymbol{T}_{q,q'} &= \sum_{i,j=1}^{n}\left(\frac{k_i'}{k}-1\right)k\boldsymbol{B}_{i,q}\wedge\boldsymbol{B}_{j,-q'}\\ &\times\left[\delta_{ij}-\left(\frac{k_j'}{k}-1\right)H_{ij}+\sum_{l=1}^{n}\left[\left(\frac{k_l'}{k}-1\right)H_{il}\right]\left[\left(\frac{k_j'}{k}-1\right)H_{lj}\right]+\cdots\right].\end{aligned}\tag{5.5}$$

At this point, it becomes necessary to define the K-matrix, whose (i,j)-th component has the form:

$$K_{ij}\equiv\left(\frac{k_j'}{k}-1\right)H_{ij}\,,\tag{5.6}$$

such that

$$\begin{aligned}\boldsymbol{T}_{q,q'} &= \sum_{i,j=1}^{n}\left(\frac{k_i'}{k}-1\right)k\boldsymbol{B}_{i,q}\wedge\boldsymbol{B}_{j,-q'}\left[\delta_{ij}-K_{ij}+\sum_{l=1}^{n}K_{il}K_{lj}+\cdots\right]\\ &= \sum_{i,j=1}^{n}\left(\frac{k_i'}{k}-1\right)k\boldsymbol{B}_{i,q}\wedge\boldsymbol{B}_{j,-q'}\left[\mathbb{I}-\boldsymbol{K}+\boldsymbol{K}^2+\cdots\right]_{i,j}.\end{aligned}\tag{5.7}$$

Recognizing the series as a geometric expansion, we can express the sum in its closed form:

$$\boldsymbol{T}_{\boldsymbol{q},\boldsymbol{q}'} = \sum_{i,j=1}^{n} \left(\frac{k_i'}{k} - 1 \right) k\boldsymbol{B}_{i,\boldsymbol{q}} \wedge \boldsymbol{B}_{j,-\boldsymbol{q}'} \left[\mathbb{I} + \boldsymbol{K} \right]^{-1}_{i,j}. \tag{5.8}$$

We have succeeded in finding a simple analytical functional form for the T-matrix, making it possible to compute its average value and apply the CPA in this more general case. It is important to note that, in this case, the H-matrix serves an analogous role to that of the function $f(k,\omega)$ in the usual CPA. However, in this context, it is an $n \times n$ matrix, where each component corresponds to the $f(k,\omega)$ function of each (i,j) interaction. We will return to the analysis of this matrix later, as it will play an important role in our theory. For now, we will continue with the generalization of the CPA, where the next step is to apply the self-consistency constraint. To do this, we need to compute the average value of the T-matrix over all possible defects, which are described by the different values that the elastic constants k_i' can take according to its probability distribution. To facilitate this calculation, we decompose the T-matrix into two distinct parts:

$$\boldsymbol{A}_{ji}^{\boldsymbol{q},\boldsymbol{q}'} \equiv k\boldsymbol{B}_{i,\boldsymbol{q}} \wedge \boldsymbol{B}_{j,-\boldsymbol{q}'}, \quad \text{and} \quad F_{ij} \equiv \left(\frac{k_i'}{k} - 1 \right) \left[\mathbb{I} + \boldsymbol{K} \right]^{-1}_{i,j}. \tag{5.9}$$

Here, $\boldsymbol{A}_{ji}^{\boldsymbol{q},\boldsymbol{q}'}$ is a $d \times d$ matrix (where d is the dimension of the lattice) given by the outer product of the i-th and j-th B-vectors, $\boldsymbol{B}_{i,\boldsymbol{q}}$ and $\boldsymbol{B}_{j,-\boldsymbol{q}'}$, respectively. Each pair (i,j) generally defines a different A-matrix, resulting in a total of n^2 distinct $d \times d$ matrices. On the other hand, F_{ij} represents the (i,j)-th component of the $n \times n$ F-matrix. Thus, we can express the T-matrix as:

$$\boldsymbol{T}_{\boldsymbol{q},\boldsymbol{q}'} = \sum_{i=1}^{n} \sum_{j=1}^{n} \boldsymbol{A}_{ji}^{\boldsymbol{q},\boldsymbol{q}'} F_{ij}. \tag{5.10}$$

Since $F_{ij} = F_{ij}(k')$ and the dependence on the defects is contained entirely within the F-matrix, the average value of the T-matrix over all possible perturbations is given by:

$$\left\langle \boldsymbol{T}_{\boldsymbol{q},\boldsymbol{q}'} \right\rangle = \sum_{i=1}^{n} \sum_{j=1}^{n} \boldsymbol{A}_{ji}^{\boldsymbol{q},\boldsymbol{q}'} \left\langle F_{ij} \right\rangle. \tag{5.11}$$

This expression shows that the mean value of the T-matrix is a linear combination

of the average values of the components of the F-matrix. Therefore, the self-consistency constraint, $\langle \boldsymbol{T}_{q,q'} \rangle = 0$, implies that the mean value of the F-matrix must vanish for every combination of (i, j):

$$\langle \boldsymbol{F} \rangle = 0 \quad \forall\, i, j. \tag{5.12}$$

Thus far, we have managed to overcome one of the greatest challenges posed by the generalization of the CPA, namely the ability to describe the sum of infinite terms in the T-matrix representation as a single term for more complex structural frameworks. Additionally, we have been able to derive analytical expressions for the matrix upon which the self-consistency constraint, in this case $\langle \boldsymbol{F} \rangle = 0$, will be applied.

In general, the H-matrix is an $n \times n$ matrix, which means that the self-consistency constraint would lead to n^2 linearly independent equations for a single variable, k. Fortunately, a deeper analysis of the H-matrix reveals that, in certain systems, the problem is not as severe as initially appears. Specifically, for the triangular lattice studied here, the symmetries and structure of the H-matrix allow for significant simplifications. By carefully examining these features, we will show that it is indeed possible to reduce and solve the self-consistency constraint. In the next section, we will explore the key features of the H-matrix in the context of the triangular lattice. These insights will demonstrate how the system's symmetries enable us to overcome this apparent obstacle, bringing us closer to a consistent and solvable formulation of the generalized CPA.

5.2 Analysis of the H-matrix in the triangular lattice

To address the self-consistency constraint effectively, we need a deeper understanding of the H-matrix defined in Eq. (5.4). Although it initially appears as a complex $n \times n$ matrix, its structure can exhibit valuable symmetries under specific conditions, such as in simple lattices like the triangular network studied here. These symmetries allow us to reduce the number of independent components, providing crucial insights into the physical meaning of the matrix elements and making the problem more tractable. While such simplifications are not universally applicable, they demonstrate that, in well-chosen systems, solving the self-consistency constraint is both feasible and well defined.

5.2.1 Diagonal components

In a homogeneous lattice, which serves as the target of mapping from the disordered system, the description in reciprocal space benefits from the rotational invariance of the system. As a result, equivalent structural elements, like the links labeled in Figure 3.2, must be described identically.

From the definition of the H-matrix in Eq. (5.4), we see that each component H_{ij} is constructed from the B-vectors of two specific links, i and j. For diagonal elements, H_{ii} involves the B-vectors of the same link i. Due to the rotational invariance of the system, the description of any other diagonal component H_{jj}, associated with a different link j, must be identical. This symmetry, while particularly evident in the triangular lattice studied here, is not exclusive to it; other lattices with similar rotational symmetries can also exhibit this simplification. However, it is important to note that such simplifications are not universally applicable and depend on the specific symmetries of the lattice under consideration.

This result significantly simplifies our formulation, since all n diagonal elements can be expressed by a single independent term, reducing the number of equations to evaluate. To further simplify the description, we rewrite the diagonal elements as

$$\begin{aligned} H_{ii} &= -k\int_{\boldsymbol{q}} d\mathbf{q}\; \boldsymbol{B}_{i,-\boldsymbol{q}} \cdot \boldsymbol{G}_{\boldsymbol{q}} \cdot \boldsymbol{B}_{i,\boldsymbol{q}} \\ &= -k\int_{\boldsymbol{q}} d\mathbf{q}\; \mathrm{tr}\Big[\big(\boldsymbol{B}_{i,\boldsymbol{q}} \wedge \boldsymbol{B}_{i,-\boldsymbol{q}}\big) \cdot \boldsymbol{G}_{\boldsymbol{q}}\Big] \\ &= -\int_{\boldsymbol{q}} d\mathbf{q}\; \mathrm{tr}\Big[\big(k\boldsymbol{B}_{i,\boldsymbol{q}} \wedge \boldsymbol{B}_{i,-\boldsymbol{q}}\big) \cdot \boldsymbol{G}_{\boldsymbol{q}}\Big]. \end{aligned} \tag{5.13}$$

Using the rotational invariance of the system, we note that the integral over the Brillouin zone will be identical for any i. This allows us to rewrite the term in parentheses as the sum

$$H_{ii} = -\int_{\boldsymbol{q}} d\mathbf{q}\; \mathrm{tr}\left[\left(\frac{1}{z_{NN}} \sum_{i=1}^{z_{NN}} k\boldsymbol{B}_{i,\boldsymbol{q}} \wedge \boldsymbol{B}_{i,-\boldsymbol{q}}\right) \cdot \boldsymbol{G}_{\boldsymbol{q}}\right], \tag{5.14}$$

where z_{NN} represents the number of links in the block. According to Eq. (3.20),

this sum is associated with the dynamical matrix, leading to:

$$H_{ii} = -\frac{1}{z_{NN}} \int_{\boldsymbol{q}} d\mathbf{q} \, \mathrm{tr}\Big[\boldsymbol{D}_{\boldsymbol{q}} \cdot \boldsymbol{G}_{\boldsymbol{q}}\Big], \tag{5.15}$$

Now, using the relation between the dynamical matrix and the zero-frequency Green's function established in Eq. (3.29), we obtain for the diagonal components of the H-matrix:

$$H_{ii} = -\frac{1}{z_{NN}} \int_{\boldsymbol{q}} d\mathbf{q} \, \mathrm{tr}\Big[\left(-\boldsymbol{G}_{\boldsymbol{q}}^{-1}\right) \cdot \boldsymbol{G}_{\boldsymbol{q}}\Big] = \frac{1}{z_{NN}} \int_{\boldsymbol{q}} d\mathbf{q} \, \mathrm{tr}\left(\mathbb{I}\right) = \frac{d}{z_{NN}}, \tag{5.16}$$

where d is the spatial dimension of the lattice. This result is significant since it not only states that all diagonal components of the H-matrix are identical, but it also provides an explicit analytical expression for them. This expression is remarkably simple, as it is given by the ratio of two well-defined constants of the system: the spatial dimension of the lattice, d, and the number of bonds per block, z_{NN}. However, it is important to note that this simplicity arises from the specific symmetries of the triangular lattice and the assumption of zero-frequency dependence. For more general lattices or systems with frequency-dependent interactions, additional considerations may be required.

A similar analysis can be extended to the off-diagonal components. By leveraging the indistinguishability of bonds in the homogeneous lattice due to the rotational invariance of the Brillouin zone, we can follow an analogous reasoning to show that all off-diagonal components of the H-matrix must also be equal to each other. This reduces the number of independent equations from n^2, as expected for an $n \times n$ matrix, to just two: one for the diagonal components and another for the off-diagonal components. Furthermore, as in the diagonal case, it is possible to derive a generalized expression for $H_{i\neq j}$ in terms of the dynamical matrix. The full derivation of this result is presented in Appendix A.

However, carrying out this full derivation for off-diagonal components may not be necessary. In the next subsection, we introduce an approximation that considers only the diagonal components of the H-matrix. This approach is particularly useful because the self-consistency constraint is ultimately employed to determine the effective elastic constant k of the homogeneous network. Since k is a

single scalar quantity, working with just one equation rather than two significantly simplifies the analysis.

If this approximation were not used, we would be left with two equations for a single unknown. A strategy to address this situation has been previously employed in similar systems, such as in the work by Mao et al. [19], where an additional term was introduced to balance the number of equations and unknowns in a triangular lattice with bending and stretching forces. In Appendix B we extend this idea. For now, we focus on the approximation that retains only the diagonal components, as it is not only more convenient but also well-justified. Moreover, we have tested numerically both approaches, and the results show no significant differences.

With this foundation established, we now turn to a detailed examination of the diagonal-only approximation, known as the non-crossing approximation. This approach relies on the assumption that interactions between pairs of defects can be neglected, simplifying the problem while retaining its essential physical features. We will discuss its underlying assumptions and the arguments that support its validity in the context of our system.

5.2.2 Non-crossing approximation

Building on the motivation outlined in the previous section, we now introduce the non-crossing approximation, which retains only the diagonal components of the H-matrix. This approximation simplifies the analysis by focusing on single-defect scattering processes while preserving the essential physics of the problem. Importantly, this does not imply neglecting correlations between disordered elements, as these will be fully incorporated through the generalized probability distribution in the self-consistency constraint. Instead, the approximation eliminates higher-order scattering processes involving interactions between pairs or clusters of defects, which are not central to our description. Our goal is to justify its validity by examining the structure of the disorder-induced perturbation matrix $\boldsymbol{V}_{q,q'}$ and its implications for phonon propagation in disordered networks.

We begin by considering the explicit form of the V-matrix, as given by Eq. (5.1):

$$\boldsymbol{V}_{q,q'} = \sum_{i=1}^{n} \boldsymbol{V}_i(\boldsymbol{q}, \boldsymbol{q}'), \tag{5.17}$$

where each term $\boldsymbol{V}_i(\boldsymbol{q}, \boldsymbol{q}')$ corresponds to a defect located at bond i in the lattice, defined as

$$\boldsymbol{V}_i(\boldsymbol{q}, \boldsymbol{q}') = (k_i' - k)\boldsymbol{B}_{i,\boldsymbol{q}} \wedge \boldsymbol{B}_{i,-\boldsymbol{q}'}. \tag{5.18}$$

In this formulation, the V-matrix contains no crossing terms. However, when examining the iterative expansion of the T-matrix,

$$\begin{aligned} \boldsymbol{T}_{q,q'} = &\sum_{i=1}^{n} \boldsymbol{V}_i(\boldsymbol{q}, \boldsymbol{q}') + \sum_{i,j=1}^{n} \int_{\boldsymbol{q}_1} d\mathbf{q}_1 \boldsymbol{V}_i(\boldsymbol{q}, \boldsymbol{q}_1) \cdot \boldsymbol{G}_{q_1} \cdot \boldsymbol{V}_j(\boldsymbol{q}_1, \boldsymbol{q}') \\ &+ \sum_{i,l,j=1}^{n} \int_{\boldsymbol{q}_1} \int_{\boldsymbol{q}_2} d\mathbf{q}_1 d\mathbf{q}_2 \boldsymbol{V}_i(\boldsymbol{q}, \boldsymbol{q}_1) \cdot \boldsymbol{G}_{q_1} \cdot \boldsymbol{V}_l(\boldsymbol{q}_1, \boldsymbol{q}_2) \cdot \boldsymbol{G}_{q_2} \cdot \boldsymbol{V}_j(\boldsymbol{q}_2, \boldsymbol{q}') + \cdots, \end{aligned} \tag{5.19}$$

we observe that higher-order terms involve interactions between pairs or clusters of defects (e.g., $i \neq j$). In the non-crossing approximation, we focus solely on single-defect scattering processes, meaning that terms involving pairs or higher-order combinations of different defects are omitted.

To clarify this assumption, we impose the following statistical condition on the defect matrices:

$$\left\langle \boldsymbol{V}_i \boldsymbol{V}_j \right\rangle = c_i \delta_{ij}, \tag{5.20}$$

where $c_i\mathbb{I}$ represents the correlation for the self-product $\boldsymbol{V}_i\boldsymbol{V}_i$. Here, the Kronecker delta δ_{ij} ensures that only single-defect contributions are retained, while terms involving interactions between different defect matrices (i.e., pairs or higher-order defect clusters) are excluded. As we will see, this property plays a crucial role in simplifying the self-consistency constraint formulated through the T-matrix.

This approximation could be best understood using diagrammatic notation for phonon scattering in disordered networks. Table 5.1 introduces the graphical representation of the relevant matrices.

Matrix	Diagrammatic Notation
$V_i(q, q')$	
G_{q_1}	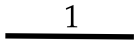

Table 5.1: Diagrammatic notation for the relevant matrices in the analysis. The defect-induced scattering matrix $V_i(q, q')$ is represented by a vertical line, while the Green's function G_{q_1}, describing phonon propagation at wavevector q_1, is represented by a horizontal line.

With this notation, we can rewrite the T-matrix expansion diagrammatically as

$$T_{q,q'} = \sum_{i=1}^{n} \quad + \sum_{i,j=1}^{n} \quad + \sum_{i,l,j=1}^{n} \quad + \cdots. \tag{5.21}$$

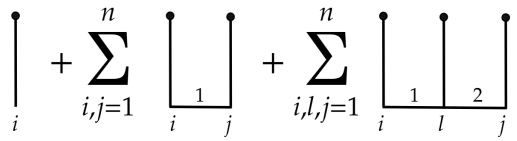

After taking the average, the non-crossing approximation further simplifies the series to only the irreducible rainbow diagrams:

$$\left\langle T_{q,q'} \right\rangle = \sum_{i=1}^{n} \quad + \sum_{i=1}^{n} \quad + \sum_{i=1}^{n} \quad + \cdots \tag{5.22}$$

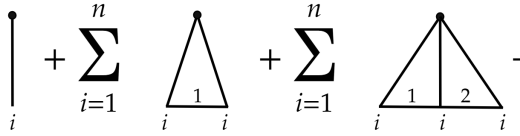

In matrix notation, this approximation reduces the T-matrix expansion to

$$\begin{aligned} T_{q,q'} = &\sum_{i=1}^{n} V_i(q, q') + \sum_{i=1}^{n} \int_{q_1} d\mathbf{q}_1 V_i(q, q_1) \cdot G_{q_1} \cdot V_i(q_1, q') \\ &+ \sum_{i=1}^{n} \int_{q_1} \int_{q_2} d\mathbf{q}_1 d\mathbf{q}_2 V_i(q, q_1) \cdot G_{q_1} \cdot V_i(q_1, q_2) \cdot G_{q_2} \cdot V_i(q_2, q') + \cdots . \end{aligned} \tag{5.23}$$

Using the definition of $V_i(q, q')$ from Eq. (5.18), we recover the diagonal form of the H-matrix,

$$H = \frac{d}{z_{NN}} \mathbb{I}, \tag{5.24}$$

which matches Eq. (5.14). This result confirms the validity of the diagonal-only approximation and justifies its use in the subsequent analysis.

It is worth reflecting on the consequences of not using this approximation.

As mentioned earlier, we would face the challenge of balancing two equations for a single unknown. While this could potentially be resolved through other methods, as described in Appendix B, the non-crossing approximation offers a simpler solution. However, it is important to note that, while this approach is well-suited for certain systems, it inherently neglects higher-order interactions that may be relevant in more complex scenarios. Therefore, before applying this approximation, it is crucial to carefully assess its validity for the specific system under study.

Now we will use the simplified description of the H-matrix in Eq. (5.24) to analyze the particular case where all bonds in the block share the same elastic constant k'. This situation is equivalent to removing entire blocks of the network with a certain probability distribution. Mathematically, this corresponds to setting $k'_i = k'$ for all i. Under the probability distribution where $k' = 1$ with a probability p and $k' = 0$ with probability $1 - p$, the self-consistency constraint takes the following form:

$$\begin{aligned}\langle \boldsymbol{F} \rangle &= p\boldsymbol{F}|_{k'=1} + (1-p)\boldsymbol{F}|_{k'=0} \\ &= p\left(\frac{1}{k} - 1\right)\left[\mathbb{I} + \left(\frac{1}{k} - 1\right)\frac{d}{z_{NN}}\mathbb{I}\right]^{-1} - (1-p)\left[\mathbb{I} - \frac{d}{z_{NN}}\mathbb{I}\right]^{-1}.\end{aligned} \tag{5.25}$$

In this diagonal case, the self-consistency constraint reduces to a single equation, which can be written as:

$$p(1-k)\left[k + \frac{d(1-k)}{z_{NN}}\right]^{-1} - (1-p)\left[1 - \frac{d}{z_{NN}}\right]^{-1} = 0. \tag{5.26}$$

From this, we recover the usual behavior [58]:

$$k = \frac{pz_{NN} - d}{z_{NN} - d}. \tag{5.27}$$

Expressed in terms of the coordination number $z = d(z_{NN}\, p)$, this becomes:

$$k = \frac{z - d^2}{d(z_{NN} - d)}. \tag{5.28}$$

For the triangular lattice, where $d = 2$ and $z_{NN} = 3$, this simplifies to:

$$k = \frac{z}{2} - 2. \tag{5.29}$$

This result will play a key role in our discussion, as it provides a direct relationship between the elastic constant k and the coordination number z for the triangular lattice.

Building on this framework, we now turn to its application in analyzing rigidity percolation in systems with spatial correlations, such as colloidal gels. These systems, with their correlated disorder, serve as an ideal test case for our generalized method. So far, we have derived a general analytical expression for the self-consistency constraint. However, the specific form of the mean value depends on the particularities of each system. In the next chapter, we will propose a strategy to model the probability distribution for such systems and apply the self-consistency constraint to study their rigidity.

Chapter 6

Simple Model with Correlated Disorder

One of the main challenges in extending the Coherent Potential Approximation (CPA) to more complex systems lies in accurately incorporating structural correlations into the effective medium theory. In this generalized framework, the calculation of the average matrix $\langle \boldsymbol{F} \rangle$ cannot follow the straightforward procedure described in Eq. (5.25), as the increased structural complexity imposes new mathematical constraints. Specifically, the dependence of the F-matrix on multiple variables introduces a coupling between terms that must be carefully addressed.

To understand this issue, let us consider the previously proposed scenario in which each k'_i can take different values determined by a predefined probability distribution. Let's assume one of the form

$$k'_i = \begin{cases} 1, & \text{with probability } p_1^i \\ 0, & \text{with probability } p_0^i \end{cases}, \tag{6.1}$$

with the normalization condition:

$$\sum_{i=1}^{n} \sum_{s=0}^{1} p_s^i = 1. \tag{6.2}$$

Based on this, the mean value of the F-matrix would be expressed as:

$$\langle \boldsymbol{F} \rangle = \sum_{i=1}^{n} \sum_{s=0}^{1} p_s^i \boldsymbol{F}|_{k'_i=s} = 0. \tag{6.3}$$

However, analyzing the form of the F-matrix in Eq. (5.9) reveals that this matrix depends on all k'_i values simultaneously. Consequently, each of its components is influenced not only by the i-th term but also by all the values of k'_i across the system. Evaluating the sum in Eq. (6.3) for a single value $k'_i = s$ neglects contributions from other terms, leading to inconclusive results.

To overcome this limitation, we propose a simple model for a configuration probability protocol. This approach shifts the perspective from assigning probabilities to individual variables k_i' to considering the configurations of the system. Taking into account all possible configurations and their associated probabilities, this method allows for the consistent calculation of $\langle \boldsymbol{F} \rangle$ while incorporating structural correlations.

In this chapter, we will detail the proposed configuration probability protocol. First, we explain how to assign probabilities to different system configurations. Then, using a triangular lattice as a model, we construct a probability protocol that accounts for the system's correlations. With these probabilities, we calculate the mean value of the F-matrix, applying the CPA to the correlated system. Finally, we use this framework to study the system's rigidity transition and analyze the results.

6.1 Configuration probabilities

To address the challenge of evaluating $\langle \boldsymbol{F} \rangle$ in systems with structural correlations, we begin by describing the possible states of the system. Each configuration will be labeled using a unique index $[\Omega]$. Consider a system where the unit cell contains n bonds, each associated with a variable k_i' that can take m possible states. In this case, there will be m^n possible configurations.

For instance, in a system like the one described earlier, where each bond can take one of two values, 0 or 1 (i.e., $m = 2$), the configurations can be organized as follows:

$$[\Omega] = \begin{cases} [1], & \text{when } k_1' = 1,\ k_2' = 1,\ k_3' = 1,\ \cdots\ k_n' = 1. \\ [2], & \text{when } k_1' = 0,\ k_2' = 1,\ k_3' = 1,\ \cdots\ k_n' = 1. \\ [3], & \text{when } k_1' = 1,\ k_2' = 0,\ k_3' = 1,\ \cdots\ k_n' = 1. \\ \vdots & \\ [2^n], & \text{when } k_1' = 0,\ k_2' = 0,\ k_3' = 0,\ \cdots\ k_n' = 0. \end{cases} \tag{6.4}$$

In this way, each possible configuration will have an associated probability $p_{[\Omega]}$.

Using this framework, the self-consistency constraint can be written as:

$$\langle \boldsymbol{F} \rangle = \sum_{\Omega=1}^{2^n} p_{[\Omega]} \boldsymbol{F}_{[\Omega]} = 0, \tag{6.5}$$

where $\boldsymbol{F}_{[\Omega]}$ represents the F-matrix evaluated for all k_i' values corresponding to the configuration $[\Omega]$. This approach ensures that every term in the sum is fully evaluated, thereby addressing the issue we faced previously.

The next challenge is to define the probabilities $p_{[\Omega]}$ associated with each configuration. The definition of these probabilities depends on the particular systems under consideration. At this stage, we will incorporate information about our correlated disordered system. To address this, in the next section, we will describe the structure of the homogeneous network using a triangular lattice and define a protocol to assign a probability to each possible configuration of the system. Additionally, in this probability calculation, we will introduce a parameterized function to quantify the degree of correlation within the system.

6.2 Probability protocol

We will now define a protocol to assign a probability to each possible configuration in a triangular lattice, as illustrated in Figure 6.1.

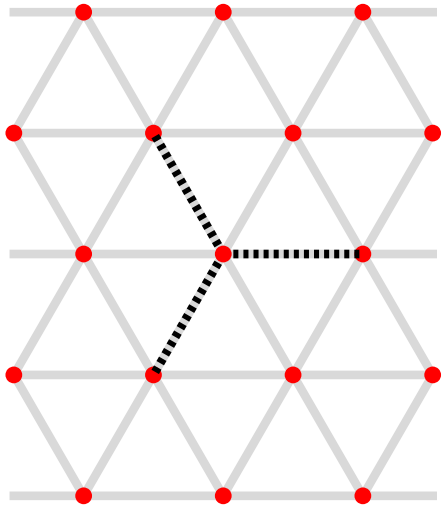

Figure 6.1: Representation of a block in a triangular lattice. The lattice sites are shown as red points, and the three links forming the block are highlighted with black dashed lines.

In this case, we define a block consisting of three links ($n = 3$), where each link can take one of two possible values for its elastic constant, k_i', namely 0 or 1. Thus, $m = 2$, resulting in a total of $2^3 = 8$ possible configurations.

To begin describing the probabilities, we start with a system where no links are present, as illustrated in Figure 6.2. We introduce a parameter p, which represents the probability that a link exists in this initial case. Using the normalization condition, the probability that a link does not exist is $1 - p$.

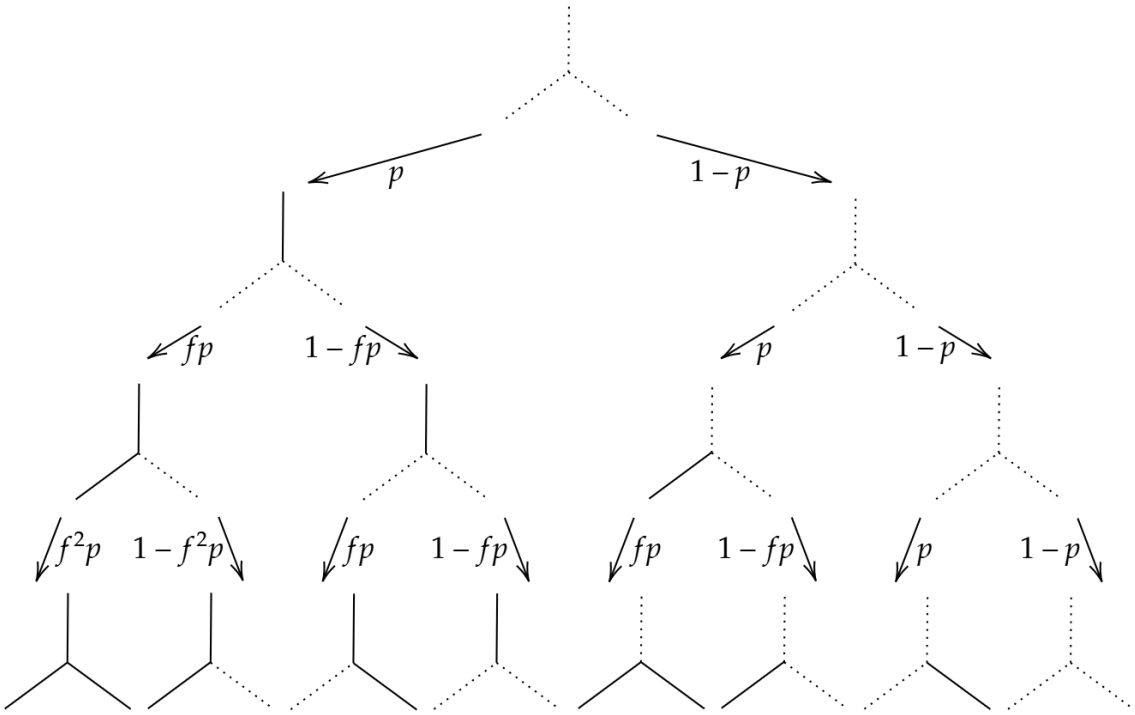

Figure 6.2: Diagram illustrating the protocol for introducing correlations in a triangular lattice block. Starting from an initial state with no links, the branching process assigns probabilities to link existence based on the parameter p and a correlation-dependent function $f = f(\alpha, p)$, where α quantifies the influence of correlations favoring link formation.

From this base system, in the leftmost branch of the diagram, we consider the scenario where one link is present. To describe the probability of a second link forming, we account for correlations in the system by introducing a function $f = f(\alpha, p)$, where α is a parameter that quantifies the influence of correlations. When $\alpha = 0$, the system has no correlations, and as α increases, the effect of correlations becomes stronger, favoring the formation of additional links in the vicinity

of existing ones. This reflects the correlated interactions we aim to describe in systems like colloidal gels. Here, $f(\alpha, p)$ acts as a modulating factor, scaling the base probability p to incorporate the influence of correlations. Thus, the probability of a second link forming, given the presence of the first, becomes $f(\alpha, p)p$, while the probability of it not forming is $1 - f(\alpha, p)p$.

It is important to note that $f(\alpha, p)$ cannot take arbitrary forms, as this could lead to inconsistencies, such as probabilities exceeding 1. We will address this constraints in the next section, where we explicitly construct $f(\alpha, p)$ to ensure it satisfies the necessary conditions for a physically meaningful description of correlated systems.

In the right branch of the first level, where no links exist initially, there is no correlation effect, so the probabilities remain p for the presence of a link and $1 - p$ for its absence.

At the second level of the leftmost branch, where two links are already present, we extend the correlation description to second-order effects. The probability of the third link forming is then $f^2(\alpha, p)p$, and the probability of it not forming is $1 - f^2(\alpha, p)p$. This second-order effect reflects the compounded influence of multiple existing links on the probability of forming additional ones.

The next branch to the right follows the same logic: if one link is already present, the probability of another forming is $f(\alpha, p)p$, and the probability of it not forming is $1 - f(\alpha, p)p$. This pattern repeats for subsequent branch.

Finally, in the rightmost branch, where no links are initially present in the unit cell, the probabilities revert to p for the presence of a link and $1 - p$ for its absence, as there are no correlations in this case.

Thus, we have constructed the 8 possible configurations for each unit cell. To obtain the probabilities associated with each configuration, we treat the construction as a joint probability by multiplying the probabilities along the branches that

lead to the desired configuration. Hence:

$$\begin{aligned}
p_{111} &= p\, fp\, f^2 p = f^3 p^3, \\
p_{110} &= p\, fp\, \left(1 - f^2 p\right) = fp^2\left(1 - f^2 p\right), \\
p_{101} &= p\, \left(1 - fp\right)\, fp = fp^2(1 - fp), \\
p_{100} &= p\, \left(1 - fp\right)\, \left(1 - fp\right) = p(1 - fp)^2, \\
p_{011} &= (1 - p)\, p\, fp = fp^2(1 - p), \\
p_{010} &= (1 - p)\, p\, \left(1 - fp\right) = p(1 - p)(1 - fp), \\
p_{001} &= (1 - p)\, (1 - p)\, p = p(1 - p)^2, \\
p_{000} &= (1 - p)\, (1 - p)\, (1 - p) = (1 - p)^3.
\end{aligned} \tag{6.6}$$

The three digits in the subscript indicate the presence or absence of links in the three unit cell elements, with 1 denoting the existence of a link and 0 its absence. From this result, it is important to analyze three key points:

1. The sum of all probabilities remains equal to one.

2. When $f(\alpha, p) = 1$, the system behaves as one without correlations. This behavior will be central in defining the form of $f(\alpha, p)$.

3. In our system, the probabilities for configurations with two links at the end are equivalent to one another, just as the probabilities for configurations with a single link at the end are also equivalent.

Then, instead of working with eight separate probability expressions, we can simplify the analysis to just four: p_3, p_2, p_1, and p_0, corresponding to configurations with three, two, one, and no links, respectively.

To express this, we compute the average of the probabilities for configurations with two links,

$$\begin{aligned}
p_2 &= \frac{1}{3}\left[fp^2\left(1 - f^2 p\right) + fp^2(1 - fp) + fp^2(1 - p)\right] \\
&= fp^2\left[1 - \frac{1}{3}p\left(f^2 + f + 1\right)\right],
\end{aligned} \tag{6.7}$$

and one link,

$$\begin{aligned} p_1 &= \frac{1}{3}\left[p(1-fp)^2 + p(1-p)(1-fp) + p(1-p)^2\right] \\ &= p\left[1 - p(f+1) + \frac{1}{3}p^2\left(f^2+f+1\right)\right], \end{aligned} \tag{6.8}$$

resulting in four probability expressions:

$$\begin{aligned} p_3 &= f^3p^3, \\ p_2 &= fp^2\left[1 - \frac{1}{3}p\left(f^2+f+1\right)\right], \\ p_1 &= p\left[1 - p(f+1) + \frac{1}{3}p^2\left(f^2+f+1\right)\right], \\ p_0 &= (1-p)^3. \end{aligned} \tag{6.9}$$

Once again, the sum of the probabilities equals one. Also, when $f(\alpha, p) = 1$, we have the expected results for a system without correlations. Now, we must develop a proper and consistent description of α and the function $f(\alpha, p)$ that captures the key characteristics of the correlations and how they influence the system.

6.3 Description of the correlation

An appropriate formulation of the function $f = f(\alpha, p)$ is essential to incorporate the correlated disorder into the system. Using this function as a modulating factor to scale the probability of link formation provides a natural starting point for modeling correlations. However, this approach alone is imprecise and can lead to inconsistencies, such as probabilities exceeding one. Although $f(\alpha, p) = 1$ eliminates correlations, its specific functional form remains undefined. It is unclear how $f(\alpha, p)$ quantifies the degree of correlation among disordered elements in the lattice or how it depends on the correlation parameter α and the base probability p, particularly when probabilities take forms like $f(\alpha, p)p$ or $f^2(\alpha, p)p$. These questions will guide our construction of the function in this section.

The protocol presented here is somewhat arbitrary, as it depends on the specific nature of the probability distribution and correlations in the system under study. Rather than providing a universal description applicable to all correlated

disordered systems, our approach aims to explore general properties and test the generalization of the CPA. In particular, the function $f(\alpha, p)$ is constructed to model a specific type of correlated behavior, but alternative forms of this modulating function—or entirely different protocols—could also be proposed depending on the system's characteristics. This flexibility highlights the adaptability of the generalized framework emphasizing that our construction is one of many possible approaches.

To refine our model and address its limitations, we propose defining the correlation parameter α subject to the following conditions:

1. α must only take positive values, as it represents the degree of correlation in the system.

2. For a system without correlations, $\alpha = 0$.

Having established these constraints, we propose a suitable construction for $f(\alpha, p)$ by imposing the following requirements:

1. $f(\alpha, p)$ must always be positive, ensuring that probabilities remain non-negative.

2. $f(\alpha, p)p$, which determines the probability along each branch where a link already exists, must not exceed 1 to avoid probabilities greater than one.

3. When $\alpha = 0$, $f(\alpha, p)$ must equal 1 to recover the non-correlated results derived in the previous section. In this case, the term $f(0, p)p$ must behave linearly, ensuring consistency with the expected behavior of the probability distribution in an uncorrelated system.

4. For $\alpha > 0$, $f(\alpha, p)p$ must be a concave downward function of p, capturing the positive effect of correlations on the probability. This concavity also ensures that, in cases of double correlation effect where the probability in the branch is given by $f^2(\alpha, p)p$, multiple correlations amplify the increase in probability.

These conditions provide a basis for constructing $f(\alpha, p)$ as a meaningful representation of correlated disorder in the system. To ensure the concave growth described in Item 4, $f(\alpha, p)p$ can be represented as a function with a $\left(\frac{\alpha}{1+\alpha p}\right) p$

behavior. Based on the conditions outlined, we propose the following formulation for the probability in each branch:

$$f(\alpha, p)p = \left(\frac{\alpha}{1+\alpha p}(1-p)+1\right)p. \tag{6.10}$$

This definition ensures that for $\alpha = 0$, the probability $f(0,p)p$ equals p, as required by Item 3. Additionally, the term $(1-p)$ guarantees that when $p = 1$, the probability does not exceed 1, thereby satisfying the constraint outlined in Item 2. Therefore, we can write an explicit and simplified form of the parameter function:

$$f(\alpha, p) = \frac{1+\alpha}{1+\alpha p}, \tag{6.11}$$

which is always positive as required in Item 1. The behavior of the probability function $f(\alpha, p)p$ as a function of p for different values of α is shown in Figure 6.3.

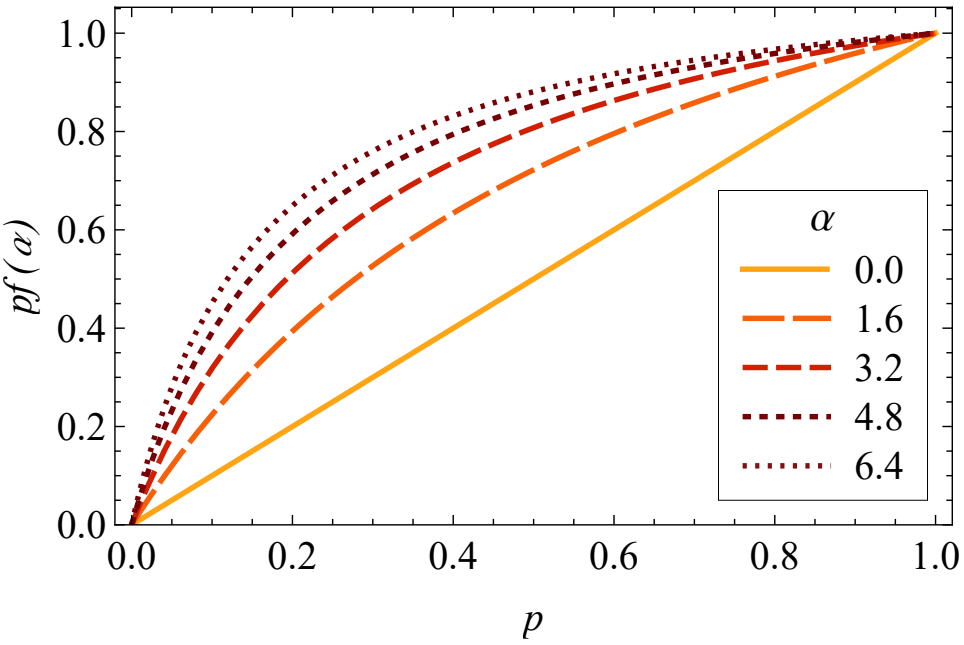

Figure 6.3: Behavior of the probability function in the branches, $pf(\alpha, p)$, as a function of the parameter p for different values of α. The uncorrelated case is represented by $\alpha = 0$ (solid line), while the correlated cases are shown for $\alpha > 0$ (dashed lines).

This figure illustrates how, for $\alpha = 0$, the function corresponds to the linear probability distribution described in the uncorrelated case. As α increases, the

probability takes a concave shape, modeling the behavior induced by correlations. Specifically, for larger α, correlations favor the presence of links, increasing the probability of a link being present at each site.

Now that this formulation meets all the necessary requirements, the function $f(\alpha, p)$ derived in Eq. (6.11) can be seamlessly incorporated into the previous description for the probabilities in Eq. (6.9).

In principle, with these probabilities, it is now possible to apply the self-consistency constraint in Eq. (6.5), allowing us to compute the mean value and find its roots to determine the values of the elastic constant of the homogeneous lattice that enable the mapping, thereby solving our system. However, there are some issues that must be addressed before proceeding with the calculations.

It is worth noting that the function $f^2(\alpha)p$ becomes greater than 1 in the interval $p \in [0, 1]$ when $\alpha > 1$. At first glance, this might seem problematic, as it implies that the probability in the doubly correlated case could exceed 1. However, this is not a problem in the final formulation, as the probability functions given in Eq. (6.9) do not exceed 1 for any α. Nevertheless, we need to address a more subtle issue that is particularly relevant for p_2: there are situations where this probability might become negative.

To better understand the behavior of these probability functions, we plot them in Figure 6.4. This figure shows the four probability functions (p_3, p_2, p_1, and p_0) as functions of the parameter p for different values of α. The solid lines represent the uncorrelated case ($\alpha = 0$), while the dashed lines correspond to correlated cases ($\alpha > 0$).

As shown in the graphic, for the uncorrelated case ($\alpha = 0$), the probabilities exhibit symmetry. When $p = 0$, the probability p_0 of having no links is 1, meaning that the system contains no links. As p increases, the probabilities of having more links grow until, at $p = 1$, the probability p_3 of having all links becomes 1. Consequently, p_0, p_1, and p_2 vanish.

In the correlated case, the general behavior is preserved, but the correlation favors link formation. As α increases, p_3 grows larger, while the other probabilities

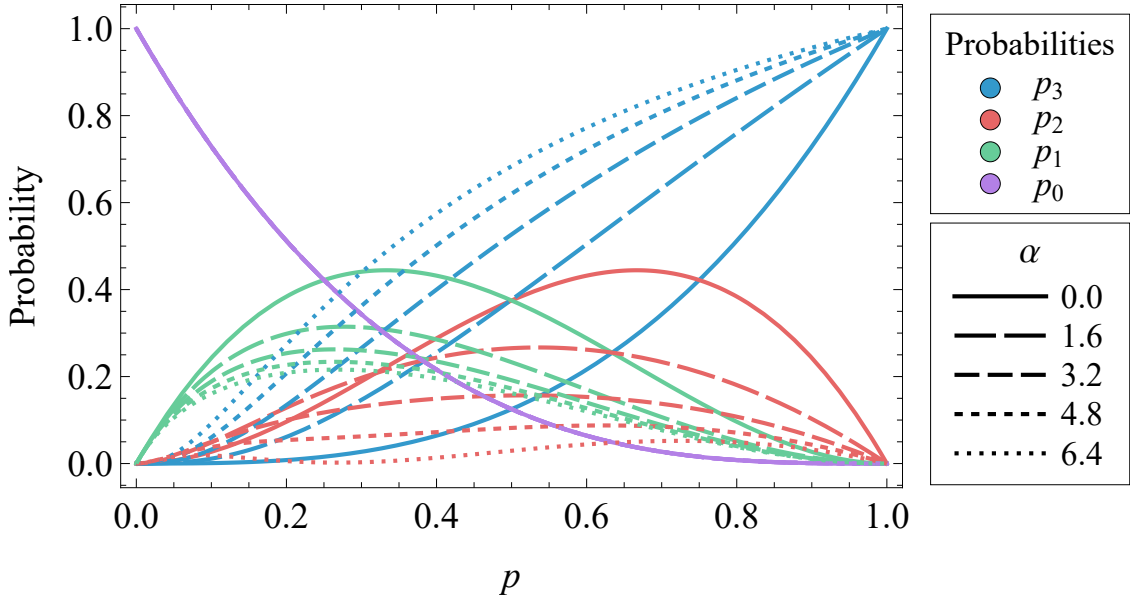

Figure 6.4: Probability functions p_0 (purple lines), p_1 (green line), p_2 (red lines), and p_3 (blue line) as functions of p for different values of α. Solid lines represent the uncorrelated case ($\alpha = 0$), while dashed lines represent correlated cases ($\alpha > 0$). Correlations increase the probability of full connectivity (p_3), reducing the probabilities of partial connectivity (p_1 and p_2), while p_0 remains unaffected by correlation.

decrease to maintain normalization. Notably, p_0 remains unchanged with correlation, as expected. This consistency arises because, with no links in the system, correlation has no effect—correlation, by definition, only affects the presence of additional links once at least one is already present.

A closer look at p_2 reveals an important feature. Given the way the probability functions in Eq. (6.9) were constructed, we observe that p_2 has two additional roots beyond the expected ones at $p = 0$ and $p = 1$. These roots become real when $\alpha^2 - 6\alpha - 3 \geq 0$, implying that p_2 could take negative values for $\alpha > 3 + 2\sqrt{3}$. In the figure, we can see how p_2 approaches zero in the region where it would eventually become negative as α approaches this upper bound.

This issue could be resolved by redefining the formulation of the probabilities. However, this is not necessary for our analysis, as it focuses on values of α typically not much greater than 1. Our primary interest is to introduce a moderate degree of correlation into the system, which can be achieved with α in the range 0.0 to 6.4. Thus, a simple upper bound on α at $3 + 2\sqrt{3}$ suffices for our purposes. For studies

involving stronger correlations, it would be necessary to redefine this protocol to ensure the physical consistency of p_2 for higher values of α.

Given this protocol and the fact that the probability of having a link is mediated by the function $f(\alpha, p)$, it is essential to highlight that the parameter p is not the probability itself. Although closely related to it, p represents the probability of having a link in the first branch of the diagram in Figure 6.2, which is the case before correlations have any effect. From that point onward, the parameter p remains closely connected to the probability, as does α, but it does not directly equal the probability of the event occurring. This distinction will be crucial for the interpretation of the results.

Finally, it is important to remember that this protocol and the probability functions in Eq. (6.9) are merely a simple model. We do not claim that these functions exactly represent the probability of link formation in correlated disordered systems, such as colloidal gels. Instead, this formulation serves as a starting point that can be adapted or redefined based on more detailed descriptions or specific information about the system under study. The protocol's flexibility allows it to evolve, depending on which aspects are most important for describing the system.

Having described this simple model to incorporate correlations within the generalized coherent potential approximation framework, we can now apply it to calculate the mean value required by the self-consistency constraint in Eq. 6.5. The logic behind the calculation is to associate the probability of each configuration in Eq. 6.9 with its corresponding F-matrix, which describes one of the eight possible configurations. After summing over all terms, we find the root of the resulting expression, which provides the value of the elastic constant k for the homogeneous lattice.

In the next section, we will implement these results numerically and analyze them in the context of rigidity percolation, studying the rigidity transition of a system with these characteristics. This numerical approach will provide insights into how correlations affect the mechanical properties of the system, offering new perspectives and potential applications.

6.4 Numerical implementation

In this section, we apply the generalized coherent potential approximation (CPA) to study the simple model inspired by colloidal gels. Our goal is to use this extended framework to study the role of correlations in rigidity transitions and analyze whether they lead to subisostatic behavior in disordered systems. To achieve this, we implement the analytical results derived throughout this document into a numerical framework, focusing on systems with correlated disorder.

We begin with a brief recap of the calculations carried out so far, emphasizing how the generalized CPA incorporates correlations through the probability protocol developed earlier. Following this, we describe the numerical implementation of these results, including the construction of the code used to solve the self-consistency constraint and compute the effective elastic constant k. The full code is provided in Appendix C.

Given the central role of symbolic manipulation in our analysis, we have used Wolfram Mathematica for its advantages in handling symbolic computations. The implementation followed these steps:

1. Definition of the Unit Cell and Vectors

    - All vectors forming the unit cell were defined. For the case of the triangular lattice shown in Figure 3.2, they take the form:

$$\boldsymbol{a}_1 = a\hat{\boldsymbol{x}}, \quad \boldsymbol{a}_2 = a\left(-\frac{1}{2}\hat{\boldsymbol{x}} + \frac{\sqrt{3}}{2}\hat{\boldsymbol{y}}\right), \quad \boldsymbol{a}_3 = a\left(-\frac{1}{2}\hat{\boldsymbol{x}} - \frac{\sqrt{3}}{2}\hat{\boldsymbol{y}}\right). \tag{6.12}$$

    - From these, the B-vectors in Eq. (3.21) were constructed, which were then used to build the total dynamical matrix of the system as the sum in Eq. (3.20).

2. Computation of the Green's Function and H-matrix

    - The dynamical matrix was used to compute the zero-frequency Green's function introduced in Eq. (3.29).

- The H_{ij} component of the H-matrix was calculated numerically by evaluating the integral in Eq. (5.4). The resulting matrix is:

$$\boldsymbol{H}_{\text{numeric}} = \begin{pmatrix} 0.666667 & -0.0465826 & -0.0465826 \\ -0.0465826 & 0.666667 & -0.0465826 \\ -0.0465826 & -0.0465826 & 0.666667 \end{pmatrix}. \tag{6.13}$$

  This matrix is constant for all values of k as discussed in Subsection 5.2.1. As expected, the diagonal components take the value $2/3$, while the off-diagonal components are a constant different from zero.

- Following the non-crossing approximation, the H-matrix can be expressed using the simplified form in Eq. (5.24). This approach eliminates the need for numerical integration. From this point onward, we will use the H-matrix with only diagonal components, which will play a key role in the discussion of the results.

3. Calculation of K- and F-Matrices

- Using the previously defined H-matrix, the K-matrix was computed according to Eq. (5.6), It is a diagonal matrix with components:

$$K_{ii}(k, k_i') = \frac{2}{3}\left(\frac{k_i'}{k} - 1\right). \tag{6.14}$$

  From this, we see that the K-matrix, depends on all k_i' values, specifically $\boldsymbol{K} = \boldsymbol{K}(k, k_1', k_2', k_3')$.

- The F-matrix was then constructed using Eq. (5.9). Its diagonal components are:

$$F_{ii} = \frac{\left(\frac{k_i'}{k} - 1\right)}{1 + \frac{2}{3}\left(\frac{k_i'}{k} - 1\right)}. \tag{6.15}$$

  This matrix serves as the T-matrix in the self-consistency constraint, where $\boldsymbol{F}(k, k_1', k_2', k_3')$ is evaluated for all possible configurations of the k_i' values according to the probability distribution.

4. Calculation of the Self-Consistency Constraint

    - The self-consistency constraint was computed using Eq. (6.5).
    - The probabilities $p_{[\Omega]}$ associated with each of the eight possible configurations were calculated using Eqs. (6.9), incorporating correlation effects through the function $f(\alpha, p)$.
    - The previously calculated F-matrix was used to associate the values of k_i' corresponding to each configuration, computing each $\boldsymbol{F}_{[\Omega]}$. Although the calculation of the mean value results in a 3×3 matrix, as discussed in Section 5.2, it is diagonal with all three components equal. Therefore, the final expression depends only on the elastic constant k and the parameters p and α; its single independent component must be set to zero to satisfy the self-consistency constraint.

Once the mean value is computed as a function of the elastic constant k and the parameters α and p, we can analyze the behavior of the elastic constant as a function of p for different values of a. This behavior is illustrated in Figure 6.5.

In this figure, it is evident that for the uncorrelated case ($\alpha = 0.0$), the expected critical behavior of rigidity percolation is recovered. Specifically, the elastic constant of the mapped homogeneous network remains zero until the critical probability $p_c = 2/3$, beyond which a phase transition to a rigid state occurs. In the rigid phase, the elastic constant becomes positive and increases continuously until reaching a value of 1 at $p = 1$. This result is consistent, as $p = 1$ corresponds to a fully connected network that contains all possible links, making it identical to a homogeneous network. Consequently, the elastic constant of the mapped homogeneous network must equal that of the disordered system, which was arbitrarily normalized to 1 in the probability distribution.

When correlations are introduced ($\alpha > 0.0$), the critical value p_c for the rigidity percolation transition decreases, as shown in Figure 6.5. This reduction is more pronounced for small values of α, while the rate of decrease slows down as α increases. Despite these changes, the expected behavior at $p = 1$ is preserved: $k = 1$ in all cases. This result is crucial, as it reflects the fact that, regardless of the correlation strength, k must equal 1 when $p = 1$, corresponding to a defect-free homogeneous lattice.

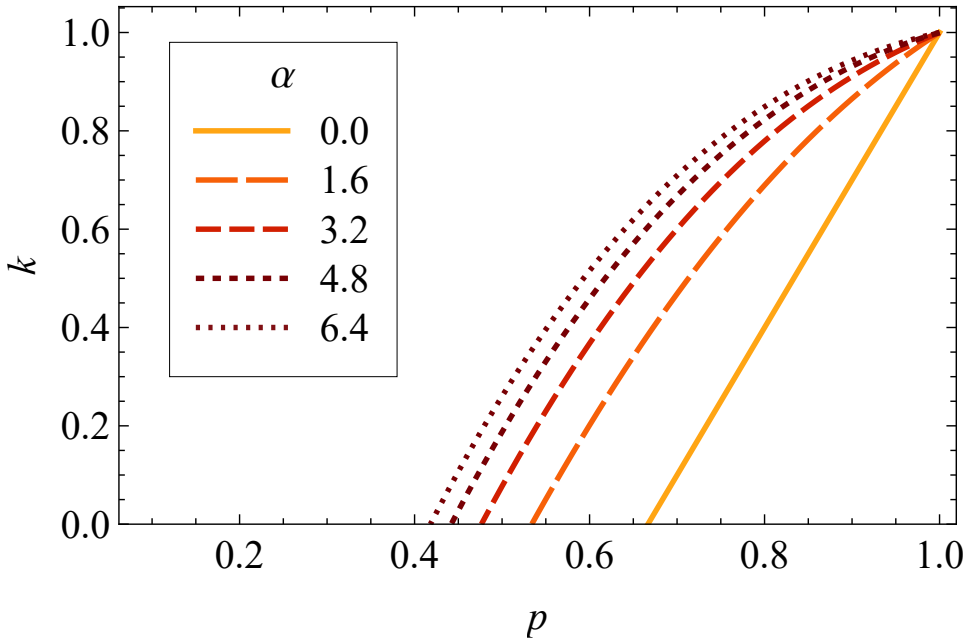

Figure 6.5: Elastic constant k as a function of link probability p for different values of the correlation parameter α. For $\alpha = 0$ (solid line), the uncorrelated system exhibits the critical behavior of rigidity percolation, where $k = 0$ for $p < 2/3$ and $k > 0$ beyond this threshold, eventually reaching $k = 1$ when $p = 1$. For $\alpha > 0$ (dashed lines), the critical threshold p_c decreases with increasing α, while k continues to approach unity at $p = 1$, as the network becomes identical to the undiluted homogeneous network in this limit. This behavior highlights the combined influence of correlation and structural contributions to rigidity.

To further analyze this behavior, we focus on the critical probability p_c as a function of α, as shown in Figure 6.6. These values are obtained by solving the self-consistency constraint for $k(p)$ at different α and determining the value of p where k becomes zero.

As seen in Figure 6.6, when $\alpha = 0$, the critical probability p_c begins at $2/3$ and decreases as α increases. This initially appears to align with subisostatic behavior, as the rigidity transition occurs for p values lower than $\frac{2}{3}$. However, as discussed in the end of Section 6.3, the parameter p, while strongly related to the probability, is not exactly equivalent to it and should not be confused with it, as the probability is modulated by a scaling function. To better understand the system's behavior, it is more reliable to analyze the elastic constant k as a function of the coordination

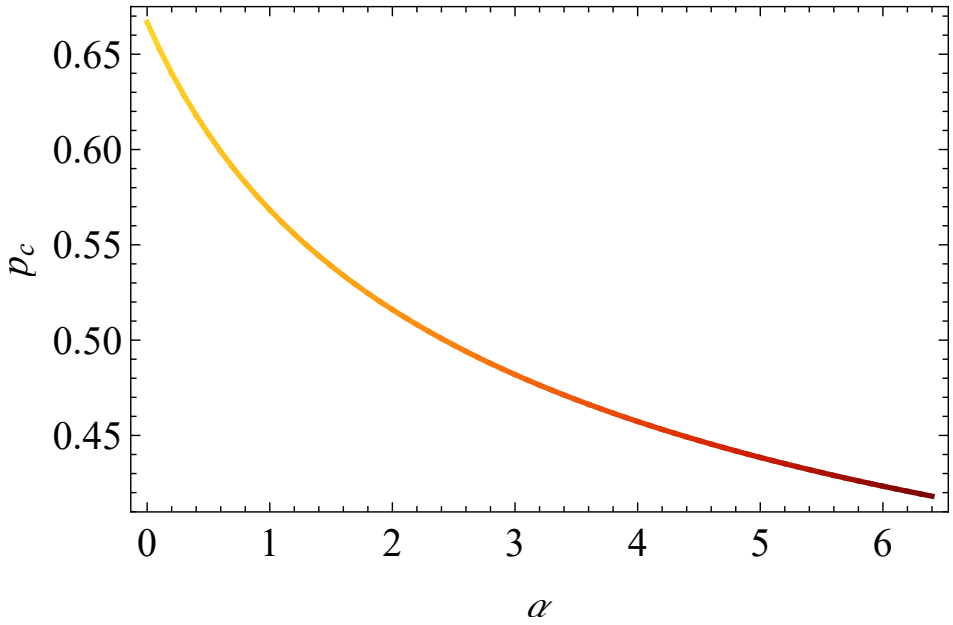

Figure 6.6: Critical probability p_c as a function of the correlation parameter α. When $\alpha = 0$, the system corresponds to the uncorrelated case, and $p_c = 2/3$, consistent with the expected rigidity percolation behavior. As α increases, p_c decreases. The decrease in p_c becomes slower as α approaches the upper limit imposed by the method of 6.4.

number z, which for our lattice can be calculated as:

$$z = d(3p_3 + 2p_2 + 1p_1 + 0p_0), \tag{6.16}$$

using the probabilities defined in Eqs. (6.9). The resulting behavior is shown in Figure 6.7.

In Figure 6.7, the correlated ($\alpha > 0$) and uncorrelated ($\alpha = 0$) cases are compared. Unlike the behavior observed in Figure 6.5, all curves converge to the same trend: the rigidity transition occurs at $z_c = 4$, as predicted by Maxwell's criterion ($z_c = 2d$). Beyond this point, k increases linearly until reaching 1 at $z = 6$, the maximum coordination number for a triangular lattice, corresponding to a fully connected network. This behavior does not exhibit the characteristics of subisostaticity, as initially suggested by Figure 6.5.

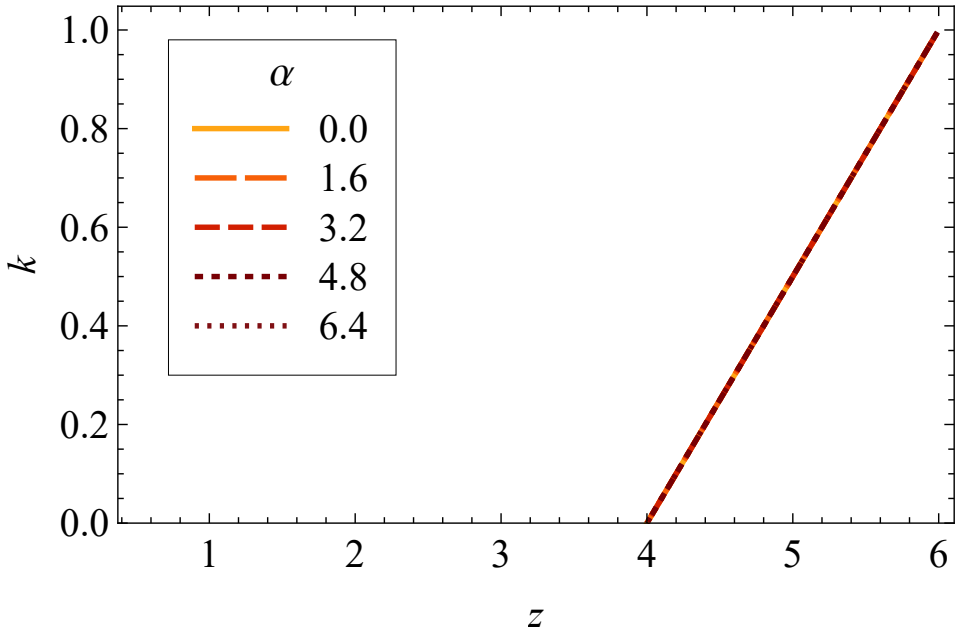

Figure 6.7: Elastic constant k as a function of the coordination number z for different values of the correlation parameter α. The $\alpha = 0$ case (solid line) represents an uncorrelated system, while the $\alpha > 0$ cases (dashed lines) correspond to correlated systems. All curves converge, with the rigidity transition occurring at $z = 4$, consistent with Maxwell's criterion ($z_c = 2d$). For $z = 6$, k reaches 1 in all cases, corresponding to the maximum coordination number in a triangular lattice.

These results highlight the importance of analyzing rigidity transitions in terms of the coordination number z, rather than the parameter p. While the initial analysis suggested subisostatic behavior, with rigidity transitions occurring at lower critical probabilities, the coordination number analysis reveals that correlations do not shift the rigidity transition below $z_c = 4$. This discrepancy raises questions about the relationship of this quantities in correlated systems. For instance, in the work by Zhang et al. [10], which studied rigidity percolation in correlated systems such as colloidal gels, it was suggested that structural correlations shift the rigidity transition to lower volume fractions. Given the relationship between volume fraction and coordination number in Eq. (2.3), one might expect a similar shift in the coordination number, implying subisostaticity. However, Zhang et al. did not directly analyze the coordination number, focusing instead on volume fractions. Our results suggest that a shift in one quantity (e.g., volume fraction or p) does not necessarily imply a corresponding shift in the coordination number, particularly in complex systems with correlated disorder.

However, it is important to note that our calculations were performed using the non-crossing approximation, as discussed in Subsection 5.2.2. This approximation neglects interactions between pairs of defects, which could contain important information about correlations, depending on the system under study. As emphasized in the introduction of the simple model for incorporating correlations into the generalized CPA framework (Section 6.3), this model is not intended to precisely describe colloidal gels. Instead, it serves as a test case for the generalized effective medium theory developed in this work. Therefore, the results should be interpreted with caution, keeping in mind the limitations of the simple model and the approximations used.

Finally, it is worth analyzing the scale invariance of our model as an indicator of the reliability of the results obtained through our generalized framework. To do this, we assume that the elastic constant k satisfies the general scaling form:

$$k = (\delta p)^f \mathcal{F}\left(\frac{\alpha}{\delta p^\varphi}\right), \tag{6.17}$$

where $\delta p = p - p_c$ is the p critical deviation, $\mathcal{F}$ is a function of $\alpha/(\delta p)^\varphi$, and f and φ are fitting parameters. Setting $f = 1$, we can rewrite this as:

$$\frac{k}{\alpha^{1/\varphi}} = \left(\frac{\delta p}{\alpha^{1/\varphi}}\right) \mathcal{F}\left(\left(\frac{\delta p}{\alpha^{1/\varphi}}\right)^{-\varphi}\right). \tag{6.18}$$

The right-hand side is a function of $\delta p/\alpha^{1/\varphi}$, allowing us to plot $k/\alpha^{1/\varphi}$ as a function of $\delta p/\alpha^{1/\varphi}$ for different values of α (excluding $\alpha = 0$ to avoid indeterminacy). By fitting φ, we find that for $\varphi = -0.15$ all curves converge, as shown in Figure 6.8.

This convergence is evidence of scale invariance in our system, suggesting universal behavior. For the fitted values of f and φ, the generalized model is consistent, and its behavior does not depend on α. This is a manifestation of scale invariance, meaning that near the critical rigidity transition point, the system's properties are independent of scale.

Another result worth analyzing is the analytical relationship between the elastic constant k and the coordination number z that our method allows us to explore.

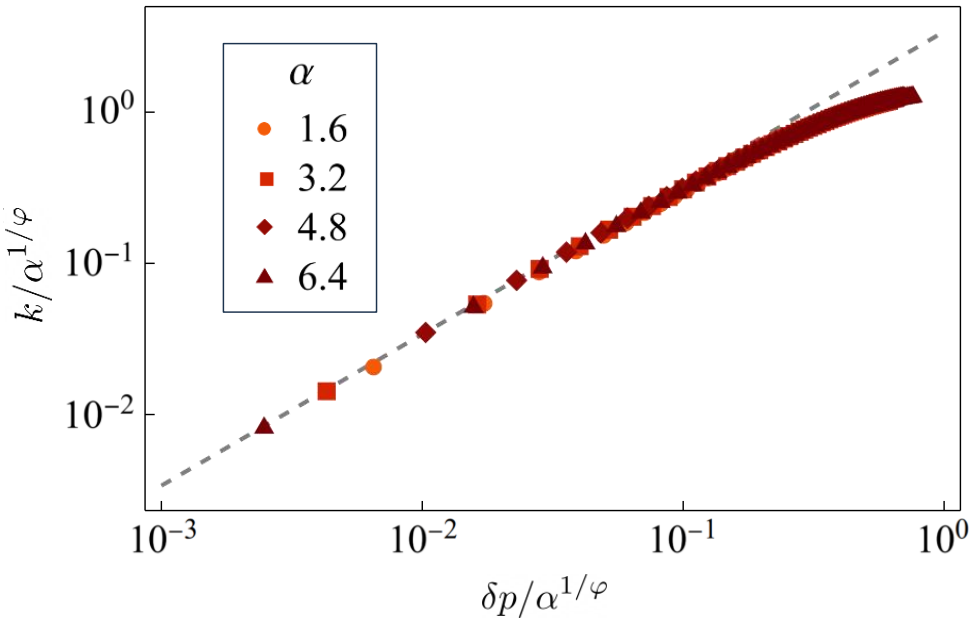

0.15

Figure 6.8: Convergence of the scaled elastic constant $k/\alpha^{1/\varphi}$ as a function of the scaled critical p deviation $\delta p/\alpha^{1/\varphi}$ for different values of α, with the fitted parameter $\varphi = -0.15$, indicating the scale invariance in the system.

By applying the self-consistency constraint numerically, we obtain the following expression for $k(\alpha, p)$:

$$k(\alpha,p) = \frac{1}{(1+p\alpha)^3}\big(-2+3p-6p\alpha+12p^2\alpha-3p^3\alpha-6p^2\alpha^2+17p^3\alpha^2 \\ -10p^4\alpha^2+2p^5\alpha^2-p^3\alpha^3+5p^4\alpha^3-4p^5\alpha^3+p^6\alpha^3\big). \tag{6.19}$$

Now, using the explicit form of $z(\alpha, p)$ given by Eq. (6.16) and using Eqs. (6.9), we have:

$$z(\alpha,p) = \frac{2}{(1+p\alpha)^3}\big(3p+12p^2\alpha-3p^3\alpha+17p^3\alpha^2 \\ -10p^4\alpha^2+2p^5\alpha^2+p^3\alpha^3+5p^4\alpha^3-4p^5\alpha^3+p^6\alpha^3\big). \tag{6.20}$$

By comparing these two expressions, we can rewrite $k(\alpha, p)$ in terms of $z(\alpha, p)$ as:

$$k(\alpha,p) = \frac{z(\alpha,p)}{2} + \frac{1}{(1+p\alpha)^3}\big(-2-6p\alpha-6p^2\alpha^2-2p^3\alpha^3\big). \tag{6.21}$$

Expanding the denominator of the second term on the right-hand side of the equation, we observe that the numerator is exactly minus twice the denominator. Thus, the relationship between k and z can be expressed as:

$$k(\alpha, p) = \frac{z(\alpha, p)}{2} - 2 \tag{6.22}$$

This is precisely the analytical expression we derived for the triangular lattice after applying the non-crossing approximation to compute the self-consistency constraint in Eq. (5.29). Moreover, it matches the behavior observed in the plot shown in Figure 6.7. From Eqs. (6.19) and (6.20), we see that both the elastic constant k and the coordination number z depend explicitly on α, reflecting the influence of correlations. However, when analyzing k as a function of z, this dependence cancels out through polynomial factorization, leaving us with a behavior that is independent of correlations.

This result demonstrates how our generalized method is capable of recovering results for the uncorrelated case while also providing insights into the role of correlations. In particular, it shows that, for systems where correlations behave as described in the simple model, the presence of correlations does not lead to subisostatic behavior.

Chapter 7

Conclusions

In this work, we have presented an analytical framework for generalizing the coherent potential approximation (CPA) to study disordered systems with complex probability distributions, including those with spatial correlations such as colloidal gels. This generalization allows us to compute the self-consistency constraint for systems where disorder is not purely independent but exhibits spatial correlations, addressing a key limitation of traditional effective medium theories.

The primary challenge in this approach lies in solving a system of n^2 linearly independent equations (n representing here the number of possible links per block), which, in general, can be computationally intractable. However, by leveraging the symmetries and specific characteristics of the system under study—such as translational invariance and the use of the non-crossing approximation—we were able to reduce the problem to a single equation. This simplification enabled us to develop a protocol for incorporating spatial correlations into the framework, using a simple model inspired by colloidal gels as a test case.

Our analysis of the rigidity transition revealed intriguing behavior. When examining the elastic constant k as a function of the link probability p, we observed that the critical threshold p_c decreased with increasing spatial correlations, suggesting a shift toward subisostatic behavior. However, a more rigorous analysis in terms of the coordination number z showed that the rigidity transition consistently occurs at $z_c = 4$, in agreement with Maxwell's criterion ($z_c = 2d$). This indicates that, while correlations alter the transition in terms of p, they do not lead to subisostatic behavior when analyzed through the lens of z. This discrepancy highlights the importance of carefully selecting the variables used to describe rigidity transitions in correlated systems. Furthermore, we demonstrated that our model exhibits scale invariance near the critical rigidity transition. This universal behavior underscores the robustness of our generalized CPA framework and its

ability to capture the essential physics of correlated disordered systems.

Despite these successes, our approach faces important challenges. The simplifications employed here, such as the non-crossing approximation, may not be applicable to all systems, particularly those with strong higher-order interactions or frequency-dependent effects. Additionally, while the simple model used in this study provides valuable insights, it is not intended to fully describe complex systems like colloidal gels. Future work will need to extend this framework to more realistic models and rigorously test its predictions against experimental data.

In conclusion, this work represents a significant step forward in the study of rigidity transitions in correlated disordered systems. By generalizing the CPA and demonstrating its applicability to a simple yet insightful model, we have laid the groundwork for future research into more complex materials. This framework has the potential to provide new insights into the mechanical properties of systems such as colloidal gels, granular materials, and biological networks, where spatial correlations play a crucial role. However, further development and validation will be essential to fully realize its potential.

Appendix A

Off-Diagonal Components of the H-matrix in the Triangular Lattice

In the main text, we demonstrated that the diagonal components of the H-matrix can be simplified significantly in the triangular lattice by leveraging the rotational invariance of the system. This invariance ensures that all diagonal elements are identical, reducing the problem to a single independent term. A natural question arises: can a similar simplification be applied to the off-diagonal components of the H-matrix?

By extending the same reasoning used for the diagonal components, we can show that the off-diagonal components also exhibit a high degree of symmetry. Specifically, the indistinguishability of bonds under rotations, dictated by the rotational invariance of the triangular lattice, implies that all off-diagonal components must be equal to each other. This further reduces the number of independent equations from n^2 to just two: one for the diagonal components and another for the off-diagonal components.

To derive an explicit expression for the off-diagonal components, we follow a procedure analogous to that used for the diagonal case. We begin by writing the general form of $H_{i\neq j}$

$$\begin{aligned} H_{i\neq j} &= -k\int_{\boldsymbol{q}} d\mathbf{q}\, \boldsymbol{B}_{i,-\boldsymbol{q}} \cdot \boldsymbol{G}_{\boldsymbol{q}} \cdot \boldsymbol{B}_{j,\boldsymbol{q}} \\ &= -\int_{\boldsymbol{q}} d\mathbf{q}\, \mathrm{tr}\Big[\left(k\boldsymbol{B}_{j,\boldsymbol{q}} \wedge \boldsymbol{B}_{i,-\boldsymbol{q}}\right) \cdot \boldsymbol{G}_{\boldsymbol{q}} \Big]. \end{aligned} \tag{A.1}$$

Using the argument of rotational invariance, we rewrite the expression in paren-

theses as a sum:

$$H_{i\neq j} = -\int_{\boldsymbol{q}} d\mathbf{q}\ \mathrm{tr}\left[\left(\frac{1}{z_{NN}}\sum_{i=1}^{z_{NN}} k\boldsymbol{B}_{i,\boldsymbol{q}} \wedge \boldsymbol{B}_{i+1,-\boldsymbol{q}}\right)\cdot \boldsymbol{G}_{\boldsymbol{q}}\right], \tag{A.2}$$

where, in the triangular lattice, all possible terms in the sum corresponding to the off-diagonal terms can be obtained from the outer products of the i-th B-vector with the $(i+1)$-th B-vector, taking into account a cyclic structure where $z_{NN}+1 \equiv 1$. This allows us to define a new matrix:

$$\hat{\boldsymbol{D}}_{\boldsymbol{q}} \equiv \sum_{m=1}^{z_{NN}} k_m \boldsymbol{B}_{m,\boldsymbol{q}} \boldsymbol{B}_{m+1,-\boldsymbol{q}'}, \tag{A.3}$$

which is constructed based on the form of the dynamical matrix. The rotational invariance of the system ensures that all terms in this sum are equivalent. Consequently, we can rewrite the off-diagonal components of the H-matrix as:

$$H_{i\neq j} = -\frac{1}{z_{NN}}\int_{\boldsymbol{q}} d\mathbf{q}\ \mathrm{tr}\left(\hat{\boldsymbol{D}}_{\boldsymbol{q}}\boldsymbol{G}_{\boldsymbol{q}}\right). \tag{A.4}$$

We have thus obtained simplified expressions for the H-matrix as well as a better understanding of its structure. Numerically, the computation becomes significantly more straightforward, as we can now write:

$$\boldsymbol{H} = -\frac{1}{z_{NN}}\int_{\boldsymbol{q}} d\mathbf{q}\left[\ \mathrm{tr}\left(\boldsymbol{D}_{\boldsymbol{q}}\boldsymbol{G}_{\boldsymbol{q}}\right)\mathbb{I} + \mathrm{tr}\left(\hat{\boldsymbol{D}}_{\boldsymbol{q}}\boldsymbol{G}_{\boldsymbol{q}}\right)(\boldsymbol{\chi}_1 - \mathbb{I})\right] \tag{A.5}$$

where $\boldsymbol{\chi}_1$ represents a matrix of all entries equal to 1, so $(\boldsymbol{\chi}_1 - \mathbb{I})$ is a matrix with zeros on the diagonal and ones on the off-diagonal. This construction ensures that the diagonal and off-diagonal components of the H-matrix are treated independently while maintaining the symmetry of the system.

The main takeaway is that the H-matrix is reduced to only two linearly independent components. This still leaves us with an important issue to address: we have two equations for a single variable, the elastic constant k of the homogeneous lattice. This problem will be discussed in Appendix B.

Appendix B

Balancing Equations in CPA

Once we have established the analytical results derived from generalizing the CPA, we encounter a particular issue during implementation. The H-matrix describing our system has two linearly independent components, both of which must satisfy the self-consistency constraint. However, within the CPA framework, we are solving for only one unknown: the elastic constant k of the homogeneous lattice, which allows us to map the disordered system. This results in a situation where we have two equations but only one unknown.

This issue has been previously encountered in similar approaches. For instance, in [19], Mao and colleagues applied effective medium theory to a triangular lattice that included bending and stretching forces. They arrived at three linearly independent terms, which had to be set to zero in a system with only two types of elastic moduli—each associated with a different type of force. To resolve this, they introduced an additional term, formulated as an auxiliary modulus that mediated an extra energy contribution resulting from the coupling of phantom bonds between next-nearest neighbors (NNN). This additional effect was modeled and incorporated into their framework, balancing the number of equations and unknowns, which allowed them to solve the problem.

This strategy aligns with the central objective of the CPA: to find an effective homogeneous medium that accurately maps the disordered system. Within this effective medium, interactions such as those involving NNN can be assumed, and the CPA can provide insights into how these interactions should behave and relate to the previously defined homogeneous elastic constant k—associated with nearest neighbors (NN). Our goal is to incorporate these additional effects into our system by directly introducing NNN interactions.

To achieve this, we will define a new unit cell with additional unit vectors, explicitly accounting for the contributions of NNN bonds, characterized by an elastic constant κ, as illustrated in Figure B.1.

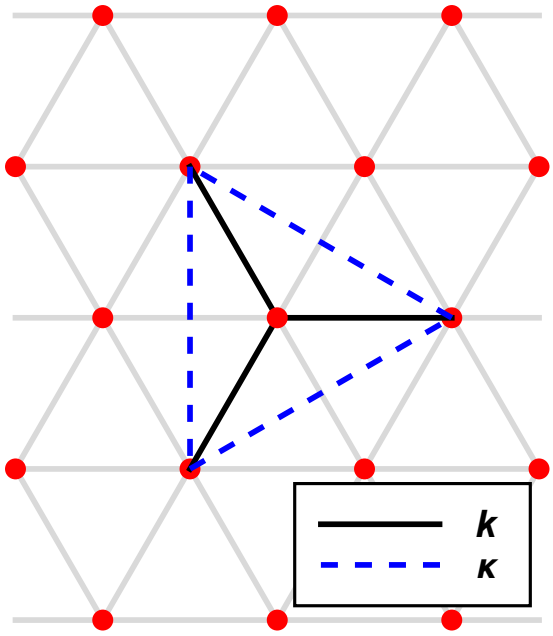

Figure B.1: Unit cell configuration illustrating nearest-neighbor interactions with elastic constant k (black solid lines) and NNN interactions with elastic constant κ (blue dashed lines).

This approach introduces the particularity of requiring the definition of three additional unit vectors in the system, which must be accounted for when calculating the dynamical matrix. We will follow the derivation in Subsection 3.2.2, in this case to calculate the $\boldsymbol{B}^{NNN}_{n,\boldsymbol{q}}$ vectors, by describing the elastic energy as a sum of all interactions d within each unit cell c mediated by the constant κ_d:

$$U_{NNN} = \sum_c \sum_d \frac{\kappa_d}{2} \left[\left(\boldsymbol{u}_{\ell^c_d} - \boldsymbol{u}_{\ell^c_{d+1}} \right) \cdot \hat{\boldsymbol{e}}_{\ell^c_d, \ell^c_{d+1}} \right]^2. \tag{B.1}$$

Here, ℓ^c_d and ℓ^c_{d+1} represent the sites connected by each NNN link, and $\hat{\boldsymbol{e}}_{\ell^c_d, \ell^c_{d+1}}$ is the new unit vector in the direction of those links. By calculating the Fourier transform, we obtain:

$$U_{NNN} = \frac{1}{2N^2} \sum_c \sum_d \kappa_d \left[\sum_{\boldsymbol{q}} \boldsymbol{u}_{\boldsymbol{q}} \left(e^{i\boldsymbol{q}\cdot\boldsymbol{r}_{\ell^c_d}} - e^{i\boldsymbol{q}\cdot\boldsymbol{r}_{\ell^c_{d+1}}} \right) \cdot \hat{\boldsymbol{e}}_{\ell^c_d, \ell^c_{d+1}} \right]^2. \tag{B.2}$$

At this point, it becomes necessary to address the vectorial part, which is

described in Figure B.2.

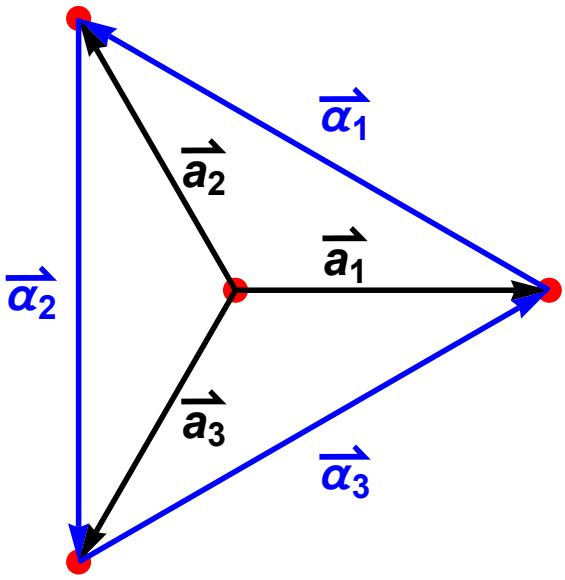

Figure B.2: Vector configuration for nearest-neighbor links, $\boldsymbol{a}_d$ (black), and next-nearest-neighbor links, $\boldsymbol{\alpha}_d$ (blue), illustrating the relationship between both sets of vectors within the unit cell.

This figure shows the vectors $\boldsymbol{a}_d$, which are associated with the NN links within the unit cell:

$$\boldsymbol{a}_1 = a\hat{\boldsymbol{x}}, \quad \boldsymbol{a}_2 = a\left(-\frac{1}{2}\hat{\boldsymbol{x}} + \frac{\sqrt{3}}{2}\hat{\boldsymbol{y}}\right), \quad \boldsymbol{a}_3 = a\left(-\frac{1}{2}\hat{\boldsymbol{x}} - \frac{\sqrt{3}}{2}\hat{\boldsymbol{y}}\right). \tag{B.3}$$

The new vectors corresponding to the NNN links will be denoted as $\boldsymbol{\alpha}_d$, and we can see that they can be constructed from the NN vectors in the following way:

$$\begin{aligned}
\boldsymbol{\alpha}_1 &= \boldsymbol{a}_2 - \boldsymbol{a}_1 = \frac{a\sqrt{3}}{2}\left(-\sqrt{3}\hat{\boldsymbol{x}} + \hat{\boldsymbol{y}}\right), \\
\boldsymbol{\alpha}_2 &= \boldsymbol{a}_3 - \boldsymbol{a}_2 = -a\sqrt{3}\hat{\boldsymbol{y}}, \\
\boldsymbol{\alpha}_3 &= \boldsymbol{a}_1 - \boldsymbol{a}_3 = \frac{a\sqrt{3}}{2}\left(\sqrt{3}\hat{\boldsymbol{x}} + \hat{\boldsymbol{y}}\right).
\end{aligned} \tag{B.4}$$

In this context, it is important to clarify the notation, as it can become confusing. For the first NNN bond, corresponding to the direction of the vector $\boldsymbol{\alpha}_1$, the two sites involved are those located at the positions defined by $\boldsymbol{a}_1$ and $\boldsymbol{a}_2$. More generally, for the d-th bond, the two sites are determined by the vectors $\boldsymbol{a}_d$ and $\boldsymbol{a}_{d+1}$, where we adopt the convention that for $d = 3$, the index $d + 1$ cycles back to

1. Thus, since in the unit cell $\boldsymbol{r}_{\ell_d^c} = \boldsymbol{r}_{\ell_0^c} + \boldsymbol{a}_d$, the elastic energy associated with the NNN links can be rewritten as:

$$U_{NNN} = \frac{1}{2N^2}\sum_c\sum_d \kappa_d \left[\sum_{\boldsymbol{q}} \boldsymbol{u}_{\boldsymbol{q}}\, e^{i\boldsymbol{q}\cdot\boldsymbol{r}_{\ell_0^c}} \left(e^{i\boldsymbol{q}\cdot\boldsymbol{a}_d} - e^{i\boldsymbol{q}\cdot\boldsymbol{a}_{d+1}}\right)\cdot \hat{\boldsymbol{e}}_{\ell_d^c,\ell_{d+1}^c}\right]^2. \tag{B.5}$$

Moreover, we can see that the unit vectors $\hat{\boldsymbol{e}}_{\ell_d^c,\ell_{d+1}^c}$ can be expressed as:

$$\begin{aligned}
\hat{\boldsymbol{e}}_{\ell_1^c,\ell_2^c} &= \frac{\boldsymbol{\alpha}_1}{|\boldsymbol{\alpha}_1|} = \frac{1}{2}\left(-\sqrt{3}\hat{\boldsymbol{x}} + \hat{\boldsymbol{y}}\right) \equiv \hat{\boldsymbol{e}}_{\alpha_1},\\
\hat{\boldsymbol{e}}_{\ell_2^c,\ell_3^c} &= \frac{\boldsymbol{\alpha}_2}{|\boldsymbol{\alpha}_2|} = -\hat{\boldsymbol{y}} \equiv \hat{\boldsymbol{e}}_{\alpha_2},\\
\hat{\boldsymbol{e}}_{\ell_3^c,\ell_1^c} &= \frac{\boldsymbol{\alpha}_3}{|\boldsymbol{\alpha}_3|} = \frac{1}{2}\left(\sqrt{3}\hat{\boldsymbol{x}} + \hat{\boldsymbol{y}}\right) \equiv \hat{\boldsymbol{e}}_{\alpha_3}.
\end{aligned} \tag{B.6}$$

Which allows us to express the energy in the form:

$$\begin{aligned}
U_{NNN} = \frac{1}{2N^2}\sum_{\boldsymbol{q},\boldsymbol{q}'} \boldsymbol{u}_{\boldsymbol{q}}\cdot\Bigg[\sum_c\sum_d \kappa_d\, e^{i(\boldsymbol{q}+\boldsymbol{q}')\cdot\boldsymbol{r}_{\ell_0^c}} \left(e^{i\boldsymbol{q}\cdot\boldsymbol{a}_d} - e^{i\boldsymbol{q}\cdot\boldsymbol{a}_{d+1}}\right)\\
\left(e^{i\boldsymbol{q}'\cdot\boldsymbol{a}_d} - e^{i\boldsymbol{q}'\cdot\boldsymbol{a}_{d+1}}\right)\hat{\boldsymbol{e}}_{\alpha_d}\hat{\boldsymbol{e}}_{\alpha_d}\Bigg]\cdot\boldsymbol{u}_{\boldsymbol{q}'}.
\end{aligned} \tag{B.7}$$

And thus, using the result from Eq. 3.13, we can describe the dynamical matrix for NNN interactions as follows:

$$\boldsymbol{D}^{NNN}_{\boldsymbol{q},\boldsymbol{q}'} = \sum_c\sum_d \kappa_d\, e^{-i(\boldsymbol{q}-\boldsymbol{q}')\cdot\boldsymbol{r}_{\ell_0^c}} \left(e^{-i\boldsymbol{q}\cdot\boldsymbol{a}_d} - e^{-i\boldsymbol{q}\cdot\boldsymbol{a}_{d+1}}\right)\left(e^{i\boldsymbol{q}'\cdot\boldsymbol{a}_d} - e^{i\boldsymbol{q}'\cdot\boldsymbol{a}_{d+1}}\right)\hat{\boldsymbol{e}}_{\alpha_d}\hat{\boldsymbol{e}}_{\alpha_d}, \tag{B.8}$$

and

$$D^{NNN}_{\boldsymbol{q}} = \sum_d \kappa_d \left(e^{-i\boldsymbol{q}\cdot\boldsymbol{a}_d} - e^{-i\boldsymbol{q}\cdot\boldsymbol{a}_{d+1}}\right)\left(e^{i\boldsymbol{q}'\cdot\boldsymbol{a}_d} - e^{i\boldsymbol{q}'\cdot\boldsymbol{a}_{d+1}}\right)\hat{\boldsymbol{e}}_{\alpha_d}\hat{\boldsymbol{e}}_{\alpha_d}. \tag{B.9}$$

From which we can define the vector

$$\boldsymbol{B}^{NNN}_{n,\boldsymbol{q}} \equiv \left(e^{-i\boldsymbol{q}\cdot\boldsymbol{a}_n} - e^{-i\boldsymbol{q}\cdot\boldsymbol{a}_{n+1}}\right)\hat{\boldsymbol{e}}_{\alpha_n}. \tag{B.10}$$

In order to express it solely in terms of n, and not $n+1$, we recall the definitions

in Eq B.4, from which $\boldsymbol{a}_{n+1} = \boldsymbol{a}_n + \boldsymbol{\alpha}_n$ Thus,

$$\boldsymbol{B}^{NNN}_{n,\boldsymbol{q}} \equiv e^{-i\boldsymbol{q}\cdot\boldsymbol{a}_n}\left(1 - e^{-i\boldsymbol{q}\cdot\boldsymbol{\alpha}_n}\right)\hat{\boldsymbol{e}}_{\alpha_n}. \tag{B.11}$$

Finally, the total dynamical matrix of the system can be expressed as

$$\boldsymbol{D}_{\boldsymbol{q}}(k,\kappa) = k\sum_m \boldsymbol{B}^{NN}_{m,\boldsymbol{q}}\boldsymbol{B}^{NN}_{m,-\boldsymbol{q}'} + \kappa\sum_n \boldsymbol{B}^{NNN}_{n,\boldsymbol{q}}\boldsymbol{B}^{NNN}_{n,-\boldsymbol{q}'}. \tag{B.12}$$

Thus, we have found a solution to the problem of insufficient unknowns in the self-consistency constraint equations.

Appendix C

Code

This appendix provides the complete Mathematica code used for the numerical implementation of the generalized coherent potential approximation (CPA) framework, as applied to the simple model inspired by colloidal gels proposed in Section 6.4. The code includes the construction of the lattice, the computation of the dynamical matrix, the Green's function, the H-matrix, and the self-consistency constraint. Additionally, it generates the plots analyzed in Section 6.4.

For better readability and organization, the full Mathematica code is provided as a separate PDF file attached to this document. This file contains the complete implementation with syntax highlighting and comments, as it appears in the Mathematica environment. The code is presented in a step-by-step manner, following the same logical structure described in the main text.

EMT with multiple bonds and different probabilities associated

Lattice Structure

Definition of the B vectors

```
Clear[em, Bm]
```
apaga

$$\text{em} = \left\{\{1, 0\}, \left\{-\frac{1}{2}, \frac{\sqrt{3}}{2}\right\}, \left\{-\frac{1}{2}, -\frac{\sqrt{3}}{2}\right\}\right\};$$

```
(*Definition of the direct vectors of the triangular lattice*)
```
definição

```
Bm[qx_, qy_] := Table[Flatten[{(1 - Exp[-I * {qx, qy}.em[[i]]) * em[[i]]}], {i, 1, 3}];
```
tabela achatar exp··· unidade imaginária

```
(*Definition of B-vectors*)
```
definição

Definition of the constants k_i', v_{BZ}, z_{NN}

```
Clear[km, vBZ, zNN]
```
apaga

```
km[k1_, k2_, k3_] := {k1, k2, k3} ;(*Definition of the vector of
```
definição

```
 values that the elastic constants can take in the probability function,
each vector corresponds to a different configuration.*)
```

$$\text{vBZ} = \frac{8\,\pi^2}{3\,\sqrt{3}};$$ `(*Volume of the Brillouin zone*)`

volume

```
zNN = 3; (*Number of links per block*)
```
número

Dynamical Matrix

```
Clear[Dynamicalmatrix, Dynamicalmatrixhat]
```
apaga

```
Dynamicalmatrix[qx_, qy_, k_] =
  FullSimplify[k Sum[Outer[Times, Bm[qx, qy][[j]], Bm[-qx, -qy][[j]]], {j, 1, 3}]];
```
simplifica comple··· s··· produ·· multiplicação

```
(*Definition of the dynamical matrix*)
```
definição

```
Dynamicalmatrixhat[qx_, qy_, k_] =
  FullSimplify[ k Outer[Times, Bm[qx, qy][[1]], Bm[-qx, -qy][[2]] +
```
simplifica complet··· produ·· multiplicação

```
    k Outer[Times, Bm[qx, qy][[2]], Bm[-qx, -qy][[3]] +
```
produ·· multiplicação

```
    k Outer[Times, Bm[qx, qy][[3]], Bm[-qx, -qy][[1]]];
```
produ·· multiplicação

```
(*Alternative definition of the dynamical matrix to be used in the
  calculation of the off-diagonal components of the H-matrix*)
```

Retarded time Green's function

```
Clear[GreensFunction]
```
apaga

```
GreensFunction[qx_, qy_, k_] := Inverse[-Dynamicalmatrix[qx, qy, k]] ;
```
matriz inversa

```
(*Definition of the Green's function*)
```
definição verde

CPA

First-Brillouin zone integration

$$12 * \frac{1}{\text{vBZ}}\ \text{NIntegrate}\left[1, \left\{qy, 0, \frac{2\pi}{3}\right\}, \left\{qx, 0, \frac{qy}{\sqrt{3}}\right\}\right];$$
integra numéricamente

```
(*Normalized integral-leveraging symmetry-over the first Brillouin zone*)
```
normalizado

Definition H-matrix numerical

```
Clear[Hii, Hij, Hmatrixnumerical];
```
apaga

```
Hii[k_?NumericQ] :=
```
expressão numérica?

$$\text{Re}\left[\text{Block}\left[\{qx, qy\}, -12 * \frac{1}{vBZ} * \frac{1}{zNN}\ \text{NIntegrate}\left[\text{Tr}[\text{Dynamicalmatrix}[qx, qy, k].\right.\right.$$
p·· bloqueia integra numé·· traço

$$\left.\left.\text{GreensFunction}[qx, qy, k]], \left\{qy, 0, \frac{2\pi}{3}\right\}, \left\{qx, 0, \frac{qy}{\sqrt{3}}\right\}\right]\right]\right];$$

```
 (*Calculation of the diagonal components of the H-matrix*)
Hij[k_?NumericQ] :=
```
expressão numérica?

$$\text{Re}\left[\text{Block}\left[\{qx, qy\}, -12 * \frac{1}{vBZ} * \frac{1}{zNN}\ \text{NIntegrate}\left[\text{Tr}[\text{Dynamicalmatrixhat}[qx, qy, k].\right.\right.$$
p·· bloqueia integra numé·· traço

$$\left.\left.\text{GreensFunction}[qx, qy, k]], \left\{qy, 0, \frac{2\pi}{3}\right\}, \left\{qx, 0, \frac{qy}{\sqrt{3}}\right\}\right]\right]\right];$$

```
 (*Calculation of the off-diagonal components of the H-matrix*)
Hmatrixnumerical[k_?NumericQ] :=
```
expressão numérica?

```
  Hii[k] × IdentityMatrix[3] + Hij[k] {{0, 1, 1}, {1, 0, 1}, {1, 1, 0}} ;
```
matriz identidade

```
 (*Construction of the H-matrix*)
```

Definition H-matrix analitical with non-crossing approximation

In[•]:=
```
Clear[Hmatrix]
```
apaga

$$\text{Hmatrix} = \left\{\left\{\frac{2}{3}, 0, 0\right\}, \left\{0, \frac{2}{3}, 0\right\}, \left\{0, 0, \frac{2}{3}\right\}\right\};$$ (*Analytical construction, after the non-crossing approximation,of the H-matrix*)

Definition of matrix K and Γ

In[•]:=
```
Clear[TableKj, Γmatrix]
```
apaga

$$\text{TableKj}[k\_, k1\_, k2\_, k3\_] = \text{Table}\left[\left(\frac{\text{km}[k1, k2, k3]\llbracket j\rrbracket}{k} - 1\right), \{i, 1, 3\}, \{j, 1, 3\}\right];$$
tabela

```
 (*Definition of the factor that will be multiplied by each element of the H-
```
definição

```
  matrix to construct the K-matrix*)
Γmatrix[k_, k1_, k2_, k3_] := Inverse[IdentityMatrix[3] +
```
matriz i··· matriz identidade

```
    Table[TableKj[k, k1, k2, k3]⟦i, j⟧ * Hmatrix⟦i, j⟧, {i, 1, 3}, {j, 1, 3}]];
```
tabela

```
 (*Using the previous definition to describe the Γ-matrix*)
```

Definition of matrix F

```
In[•]:= Clear[TableKi, Fmatrix];
        apaga
        TableKi[k_, k1_, k2_, k3_] = Table[(km[k1, k2, k3][[i]]/k - 1), {i, 1, 3}, {j, 1, 3}];
                                     tabela
        (*Definition of the factor that will be multiplied by each element of the Γ-
          definição
         matrix to construct the F-matrix*)
        Fmatrix[k_, k1_, k2_, k3_] :=
          Table[TableKi[k, k1, k2, k3][[i, j]] * Γmatrix[k, k1, k2, k3][[i, j]], {i, 1, 3}, {j, 1, 3}];
          tabela
        (*Definition of the F-matrix*)
          definição
```

Probabilities protocol

Definition of the probabilities

```
Clear[p0, p1, p2, p3, f]
apaga
f[p_, α_] := (1 + α)/(1 + α p);
p3[p_, α_] := (f[p, α])^3 p^3;
p2[p_, α_] := (f[p, α]) p^2 (1 - 1/3 p ((f[p, α])^2 + (f[p, α]) + 1));
p1[p_, α_] := p (1 - p ((f[p, α]) + 1) + 1/3 p^2 ((f[p, α])^2 + (f[p, α]) + 1));
p0[p_, α_] := (1 - p)^3;
(*Definition of the probability protocol
  definição
 using the definition of the function f(α,p)*)
```

CPA self-consistency equation

```
In[•]:= Clear[MeanValueFmatrix]
        apaga
        MeanValueFmatrix[p_, α_, k_] :=
          p3[p, α] × Fmatrix[k, 1, 1, 1] + p2[p, α] × Fmatrix[k, 1, 1, 0] +
           p2[p, α] × Fmatrix[k, 1, 0, 1] + p2[p, α] × Fmatrix[k, 0, 1, 1] +
           p1[p, α] × Fmatrix[k, 1, 0, 0] + p1[p, α] × Fmatrix[k, 0, 1, 0] +
           p1[p, α] × Fmatrix[k, 0, 0, 1] + p0[p, α] × Fmatrix[k, 0, 0, 0];
        (*Calculation of the mean value of the F-
         matrix:Each probability is multiplied by the F-matrix associated with each
            configuration of the elastic constants k'_i values in the block*)
```

Solutions of the self-consistency constraint

Plot k(p) varying α

In[•]:=
```
ps = Reverse[Table[x, {x, 0.1, 0.99, 0.01}]];
(*Definition of the values of the parameter p that will be plotted*)
αs = Table[x, {x, 0.0, 3 + 2 * √3, 1.6}];
(*Definition of the values of the parameter α that will be plotted*)
tabplotkp = {}; (*Initialization of the table where the results will be stored*)
For[i = 1, i ≤ Length[αs], i++, (*For loop for each plot of α*)
 αv = αs[[i]];
 cadagraph = {}; (*Initialization of the table where the results will be stored*)
 k0 = 0.9; (*Value of the initial guess to be used in FindRoot where the self-
  consistency constraint will be calculated*)
 For[j = 1, j ≤ Length[ps], j++, (*For loop for each value of p*)
   pv = ps[[j]];
   kv = k /. FindRoot[MeanValueFmatrix[pv, αv, k][[1, 1]] == 0, {k, k0}];
   (*Obtaining the elastic constant k through the application of the self-
    consistency constraint*)
   AppendTo[cadagraph, {pv, kv}]; (*Storage of the obtained results*)
   k0 = kv; (*Update of the initial guess for the next loop*)
  ] ×
 AppendTo[tabplotkp, cadagraph]; (*Storage of the obtained results*)
]
```

Plot k(z) varying α

In[•]:=
```
ps = Reverse[Table[x, {x, 0.1, 0.99, 0.01}]];
(*Definition of the values of the parameter p that will be plotted*)
αs = Table[x, {x, 0.0, 3 + 2 Sqrt[3], 1.6}];
(*Definition of the values of the parameter α that will be plotted*)
tabplotkz = {}; (*Initialization of the table where the results will be stored*)

For[i = 1, i ≤ Length[αs], i++, (*For loop for each plot of α*)
 αv = αs[[i]];
 cadagraphz = {}; (*Initialization of the table where the results will be stored*)
 k0 = 0.9; (*Value of the initial guess to be used in FindRoot where the self-
  consistency constraint will be calculated*)
 For[j = 1, j ≤ Length[ps], j++, (*For loop for each value of p*)
  pv = ps[[j]];
  kv = k /. FindRoot[MeanValueFmatrix[pv, αv, k][[1, 1]] == 0, {k, k0}];
  (*Obtaining the elastic constant k through the application of the self-
   consistency constraint*)
  zv = 2 (3 p3[pv, αv] + 2 × 3 p2[pv, αv] + 3 p1[pv, αv]);
  (*Calculation of the coordination number z*)
  AppendTo[cadagraphz, {zv, kv}]; (*Storage of the obtained results*)
  k0 = kv;]; (*Update of the initial guess for the next cycle*)
 AppendTo[tabplotkz, cadagraphz];] (*Storage of the obtained results*)
```

Plot $p_c(\alpha)$

```
Clear[ps, αp, tabcriticalpoints, cadagraphcp]
ps = Reverse[Table[x, {x, 0.1, 0.99, 0.01}]];
(*Definition of the values of the parameter p that will be plotted*)
αp = Table[x, {x, 0.0, 3 + 2 * √3, 0.1}];
(*Definition of the values of the parameter α that will be plotted,
more than in previous cases*)
```

```
tabcriticalpoints = {};
(*Initialization of the table where the results will be stored*)
  inicialização
For[i = 1, i ≤ Length[αp], i++, (*For loop for each plot of α*)
para cada      comprimento      para cada
 αv = αp[[i]];
 cadagraphcp = {};
 (*Initialization of the table where the results will be stored*)
   inicialização
 k0 = 0.9; (*Value of the initial guess to be used in FindRoot where the self-
                                                        encontra raiz
  consistency constraint will be calculated*)
 For[j = 1, j ≤ Length[ps], j++, (*For loop for each value of p*)
para cada      comprimento      para cada
   pv = ps[[j]];
   kv = k /. FindRoot[MeanValueFmatrix[pv, αv, k][[1, 1]] == 0, {k, k0}];
            encontra raiz
   (*Obtaining the elastic constant k through the application of the self-
    consistency constraint*)
   AppendTo[cadagraphcp, {pv, kv}]; (*Storage of the obtained results*)
    adiciona a
   k0 = kv; (*Update of the initial guess for the next cycle*)
             atualiza
  ] ×
  AppendTo[tabcriticalpoints, cadagraphcp]; (*Storage of the obtained results*)
   adiciona a
]
criticalPoints = {};
(*Initialization of the table where the results will be stored*)
  inicialização
For[i = 1, i ≤ Length[tabcriticalpoints], i++,
para cada      comprimento
  cadagraphcp = tabcriticalpoints[[i]]; (*For loop for each critical point*)
                                          para cada
  interpolation = Interpolation[cadagraphcp];
                  interpolação
  (*Interpolation to find a more accurate zero*)
    interpolação
  pc = x /. FindRoot[interpolation[x] == 0, {x, 0.67}];
           encontra raiz
  (*Calculation of the critical point of p*)
  AppendTo[criticalPoints, {αp[[i]], pc}];]; (*Storage of the obtained results*)
   adiciona a
```

Scale Invariance

```
interpolations = {};
(*Initialization of the table where the results will be stored*)
shiftedInterpolations = {};
(*Initialization of the table where the results will be stored*)
graphs = {}; (*Initialization of the table where the results will be stored*)
allShiftedData = {};
(*Initialization of the table where the results will be stored*)
For[i = 1, i ≤ Length[tabplotkp], i++,
  cadagraph = tabplotkp[[i]]; (*For loop for each previous result*)
  interpolation = Interpolation[cadagraph];
  (*Interpolation to find a more accurate zero*)
  AppendTo[interpolations, interpolation]; (*Storage of the obtained results*)
  pc = x /. FindRoot[interpolation[x] == 0, {x, 0.67}];
  (*Calculation of the critical point of p*)
  shiftedData = {};
  (*Initialization of the table where the results will be stored*)
  For[j = 1, j ≤ Length[cadagraph], j++, (*For loop for each graph*)
   shiftedpv = cadagraph[[j, 1]] - pc; (*Definition of Δp*)
   kv = cadagraph[[j, 2]];
   If[kv > 0, AppendTo[shiftedData, {shiftedpv, kv}]];
   (*Storage of the positive obtained results*)
  ];
  AppendTo[allShiftedData, shiftedData]; (*Storage of the obtained results*)
 ];
```

Fitting parameters f and ϕ

```
Clear[scaledData]
scaledData[rawData_, ϕ_] :=
  Table[Table[{rawData[[i]][[j, 1]]/αs[[i]]^ϕ, rawData[[i]][[j, 2]]/αs[[i]]^ϕ}, {j, 1, Length[rawData[[i]]]}],
   {i, 2, Length[αs]}]; (*Fitting process of the parameter ϕ*)
```

```
Manipulate[ListLogLogPlot[scaledData[allShiftedData, ϕ]], {ϕ, -0.15, 0}]
```
manipula gráfico log–log de uma lista de valores

```
(*Manipulate to find the fittest phi*)
```
manipula

```
Clear[scaledDataforf]
```
apaga

```
scaledDataforf[rawData_, f_] :=
  Table[Table[{rawData[[i]][[j, 1]], (rawData[[i]][[j, 2]])^f}, {j, 1, Length[rawData[[i]]]}],
    {i, 2, Length[αs]}]; (*Fitting process of the parameter f*)
```
tabela tabela comprimento comprimento

```
Manipulate[ListLogLogPlot[scaledDataforf[allShiftedData, f]], {f, 0, 1}];
```
manipula gráfico log–log de uma lista de valores

```
(*Manipulate to find the fittest f*)
```
manipula

Bibliography

[1] N. W. Ashcroft and N. D. Mermim. *Solid State Physics*. Cornell University, 1976.

[2] C. Kittel. *Introduction to Solid State Physics*. John Wiley & Sons, 8th edition, 2004.

[3] M. F. Thorpe. Continuous deformations in random networks. *Journal of Non-Crystalline Solids*, 57(3):355–370, 1983.

[4] S. Alexander. Amorphous solids: their structure, lattice dynamics and elasticity. *Physics reports*, 296(2-4):65–236, 1998.

[5] T. Matsunaga, T. Sakai, Y. Akagi, U. I. Chung, and M. Shibayama. Structure characterization of tetra-PEG gel by small-angle neutron scattering. *Macromolecules*, 42(4):1344–1351, 2009.

[6] W. Richtering and B. R. Saunders. Gel architectures and their complexity. *Soft Matter*, 10:3695, 2014.

[7] J. L. Barrat, E. Del Gado, S. U. Egelhaaf, X. Mao, M. Dijkstra, D. J. Pine, S. K. Kumar, K. Bishop, O. Gang, A. Obermeyer, et al. Soft matter roadmap. *Journal of Physics: Materials*, 7(1):012501, 2023.

[8] J. C. Maxwell. L. on the calculation of the equilibrium and stiffness of frames. *The London, Edinburgh, and Dublin Philosophical Magazine and Journal of Science*, 27(182):294–299, 1864.

[9] C. P. Broedersz, X. Mao, T. C. Lubensky, and F. C. MacKintosh. Criticality and isostaticity in fibre networks. *Nature Physics*, 7(12):983–988, 2011.

[10] S. Zhang, L. Zhang, M. Bouzid, D. Z. Rocklin, E. Del Gado, and X. Mao. Correlated rigidity percolation and colloidal gels. *Phys. Rev. Lett.*, 123:058001, 2019.

[11] S. Feng, M. F. Thorpe, and E. Garboczi. Effective-medium theory of percolation on central-force elastic networks. *Physical Review B*, 31(1):276, 1985.

[12] X. Mao, N. Xu, and T. C. Lubensky. Soft modes and elasticity of nearly isostatic lattices: Randomness and dissipation. *Physical review letters*, 104(8):085504, 2010.

[13] H. W. Haslach Jr. *Random heterogeneous materials: microstructure and macroscopic properties*, volume 55. American Society of Mechanical Engineers, 2002.

[14] V. K. de Souza and P. Harrowell. Rigidity Percolation and the spatial heterogeneity of soft modes in disordered materials. *Proceedings of the National Academy of Sciences*, 106(36):15136–15141, 2009.

[15] S. Zhang, E. Stanifer, V. V. Vasisht, L. Zhang, E. Del Gado, and X. Mao. Prestressed elasticity of amorphous solids. *Physical Review Research*, 4(4):043181, 2022.

[16] D. J. Jacobs and M. F. Thorpe. Generic rigidity percolation: the pebble game. *Physical review letters*, 75(22):4051, 1995.

[17] M. Das, F. C. MacKintosh, and A. J. Levine. Effective medium theory of semiflexible filamentous networks. *Physical review letters*, 99(3):038101, 2007.

[18] C. Heussinger, B. Schaefer, and E. Frey. Nonaffine rubber elasticity for stiff polymer networks. *Physical Review E*, 76(3):031906, 2007.

[19] X. Mao, O. Stenull, and T. C. Lubensky. Effective-medium theory of a filamentous triangular lattice. *Physical Review E*, 87(4):042601, 2013.

[20] A. J. Liu and S. R. Nagel. Jamming is not just cool any more. *Nature*, 396(6706):21–22, 1998.

[21] A. J. Liu and S. R. Nagel. The jamming transition and the marginally jammed solid. *Annual Review of Condensed Matter Physics*, 1(1):347–369, 2010.

[22] M. Wyart. On the rigidity of amorphous solids. *Annales de Physique*, 30:1–96, 2005.

[23] A. V. Tkachenko and T. A. Witten. Stress propagation through frictionless granular material. *Physical review E*, 60(1):687, 1999.

[24] S. F. Edwards and D. V. Grinev. Statistical mechanics of stress transmission in disordered granular arrays. *Physical review letters*, 82(26):5397, 1999.

[25] A. J. Rader, B. M. Hespenheide, L. A. Kuhn, and M. F. Thorpe. Protein unfolding: rigidity lost. *Proceedings of the National Academy of Sciences*, 99(6):3540–3545, 2002.

[26] J. Wilhelm and E. Frey. Elasticity of stiff polymer networks. *Physical review letters*, 91(10):108103, 2003.

[27] J. C. Phillips. Topology of covalent non-crystalline solids ii: Medium-range order in chalcogenide alloys and a-si (ge). *Journal of Non-Crystalline Solids*, 43(1):37–77, 1981.

[28] J. C. Phillips and M. F. Thorpe. Constraint theory, vector percolation and glass formation. *Solid State Communications*, 53(8):699–702, 1985.

[29] H. He and M. F. Thorpe. Elastic properties of glasses. *Physical Review Letters*, 54(19):2107, 1985.

[30] M. F. Thorpe, D. J. Jacobs, M. V. Chubynsky, and J. C. Phillips. Self-organization in network glasses. *Journal of Non-Crystalline Solids*, 266:859–866, 2000.

[31] P. A. Janmey, S. Hvidt, J. Lamb, and T. P. Stossel. Resemblance of actin-binding protein/actin gels to covalently crosslinked networks. *Nature*, 345(6270):89–92, 1990.

[32] F. C. MacKintosh, J. Käs, and P. A. Janmey. Elasticity of semiflexible biopolymer networks. *Physical review letters*, 75(24):4425, 1995.

[33] D. A. Head, A. J. Levine, and F. C. MacKintosh. Deformation of cross-linked semiflexible polymer networks. *Physical review letters*, 91(10):108102, 2003.

[34] D. A. Head, A. J. Levine, and F. C. MacKintosh. Mechanical response of semiflexible networks to localized perturbations. *Physical Review E*, 72(6):061914, 2005.

[35] C. Stormand, J. J. Pastore, F. C. MacKintosh, T. C Lubensky, and P. A. Janmey. Nonlinear elasticity in biological gels. *Nature*, 435(7039):191–194, 2005.

[36] P. R. Onck, T. Koeman, T. Van Dillen, and E. van der Giessen. Alternative explanation of stiffening in cross-linked semiflexible networks. *Physical review letters*, 95(17):178102, 2005.

[37] K. E. Kasza, A. C. Rowat, J. Liu, T. E. Angelini, C. P. Brangwynne, G. H. Koenderink, and D. A. Weitz. The cell as a material. *Current opinion in cell biology*, 19(1):101–107, 2007.

[38] E. M. Huisman and T. C. Lubensky. Internal stresses, normal modes, and nonaffinity in three-dimensional biopolymer networks. *Physical review letters*, 106(8):088301, 2011.

[39] M. Kleman and O. D. Lavrentovich. Soft matter physics: an introduction. *Springer Science Business Media*, 2007.

[40] M. Bouzid and E. Del Gado. Network topology in soft gels: Hardening and softening materials. *Langmuir*, 34(3):773–781, 2018.

[41] K. A. Whitaker, Z. Varga, L. C. Lilian, et al. Colloidal gel elasticity arises from the packing of locally glassy clusters. *Nat Commun*, 10:2237, 2019.

[42] C. R. Calladine. Buckminster fuller's "tensegrity" structures and clerk maxwell's rules for the construction of stiff frames. *International journal of solids and structures*, 14(2):161–172, 1978.

[43] S. Pellegrino and C. R. Calladine. Matrix analysis of statically and kinematically indeterminate frameworks. *International Journal of Solids and Structures*, 22(4):409–428, 1986.

[44] M. Wyart, H. Liang, A. Kabla, and L. Mahadevan. Elasticity of floppy and stiff random networks. *Physical review letters*, 101(21):215501, 2008.

[45] D. J. Jacobs and B. Hendrickson. An algorithm for two-dimensional rigidity percolation: the pebble game. *Journal of Computational Physics*, 137(2):346–365, 1997.

[46] J. C. Phillips. Topology of covalent non-crystalline solids I: Short-range order in chalcogenide alloys. *Journal of non-crystalline solids*, 34(2):153—181, 1979.

[47] E. Guyon, S. Roux, A. Hansen, D. Bideau, J. P. Troadec, and H. Crapo. Non-local and non-linear problems in the mechanics of disordered systems: application to granular media and rigidity problems. *Reports on Progress in Physics*, 53(4):373, 1990.

[48] S. Feng and P. N. Sen. Percolation on elastic networks: new exponent and threshold. *Physical review letters*, 52(3):216, 1984.

[49] L. E. Silbert, A. J. Liu, and S. R. Nagel. Vibrations and diverging length scales near the unjamming transition. *Physical review letters*, 95(9):098301, 2005.

[50] N. Xu, M. Wyart, A. J. Liu, and S. R. Nagel. Excess vibrational modes and the boson peak in model glasses. *Physical review letters*, 98(17):175502, 2007.

[51] N. Xu, V. Vitelli, M. Wyart, A. J. Liu, and S. R. Nagel. Energy transport in jammed sphere packings. *Physical review letters*, 102(3):038001, 2009.

[52] A. Souslov, A. J. Liu, and T. C. Lubensky. Elasticity and response in nearly isostatic periodic lattices. *Physical review letters*, 103(20):205503, 2009.

[53] D. J. Durian. Foam mechanics at the bubble scale. *Physical review letters*, 75(26):4780, 1995.

[54] C. S. O'Hern, S. A. Langer, A. J. Liu, and S. R. Nagel. Random packings of frictionless particles. *Physical Review Letters*, 88(7):075507, 2002.

[55] C. S. O'Hern, L. E. Silbert, A. J. Liu, and S. R. Nagel. Jamming at zero temperature and zero applied stress: The epitome of disorder. *Physical Review E*, 68(1):011306, 2003.

[56] D. B. Liarte, S. J. Thornton, E. Schwen, I. Cohen, D. Chowdhury, and J. P. Sethna. Universal scaling for disordered viscoelastic matter near the onset of rigidity. *Physical Review E*, 106(5):L052601, 2022.

[57] D. B. Liarte, X. Mao, O. Stenull, and T. C. Lubensky. Jamming as a multicritical point. *Phys. Rev. Lett.*, 122:128006, 2019.

[58] D. B. Liarte, O. Stenull, and T. C. Lubensky. Multifunctional twisted kagome lattices: Tuning by pruning mechanical metamaterials. *Phys. Rev. E.*, 101:063001, 2020.

[59] E. J. Garboczi and M. F. Thorpe. Effective-medium theory of percolation on central-force elastic networks. iii. the superelastic problem. *Physical Review B*, 33(5):3289, 1986.

[60] P. Boolchand, D. G. Georgiev, and B. Goodman. Discovery of the intermediate phase in chalcogenide glasses. *Journal of Optoelectronics and Advanced Materials*, 3(3):703–720, 2001.

[61] W. G. Ellenbroek, V. F. Hagh, A. Kumar, M. F. Thorpe, and M. Van Hecke. Rigidity loss in disordered systems: Three scenarios. *Physical review letters*, 114(13):135501, 2015.

[62] D. J. Koeze and B. P. Tighe. Sticky matters: Jamming and rigid cluster statistics with attractive particle interactions. *Physical review letters*, 121(18):188002, 2018.

[63] S. Manley, L. Cipelletti, V. Trappe, A. E. Bailey, R. J. Christianson, U. Gasser, V. Prasad, P. N. Segre, M. P. Doherty, S. Sankaran, et al. Limits to gelation in colloidal aggregation. *Physical review letters*, 93(10):108302, 2004.

[64] P. J. Lu, E. Zaccarelli, F. Ciulla, A. B. Schofield, F. Sciortino, and D. A. Weitz. Gelation of particles with short-range attraction. *Nature*, 453(7194):499–503, 2008.

[65] V. Trappe, V. Prasad, L. Cipelletti, P. N. Segre, and D. A. Weitz. Jamming phase diagram for attractive particles. *Nature*, 411(6839):772–775, 2001.

[66] T. A. Witten and P. Pincus. *Structured fluids: polymers, colloids, surfactants*. Oxford University Press, 2004.

[67] J. P. Hansen and I. R. McDonald. *Theory of simple liquids: with applications to soft matter*. Academic press, 2013.

[68] D. Richard, J. Hallett, T. Speck, and C. P. Royall. Coupling between criticality and gelation in "sticky" spheres: A structural analysis. *Soft Matter*, 14(27):5554–5564, 2018.

[69] M. Lax. Multiple scattering of waves. *Reviews of Modern Physics*, 23(4):287, 1951.

[70] R. J. Elliott, J. A. Krumhansl, and P. L. Leath. The theory and properties of randomly disordered crystals and related physical systems. *Reviews of modern physics*, 46(3):465, 1974.

[71] P. Soven. Contribution to the theory of disordered alloys. *Physical Review*, 178(3):1136, 1969.

[72] D. W. Taylor. Vibrational properties of imperfect crystals with large defect concentrations. *Physical Review*, 156(3):1017, 1967.

[73] G. B Arfken, H. J. Weber, and F. E. Harris. *Mathematical Methods for Physicists*. Academic Press, 7 edition, 2012.

[74] E. J. Garboczi and M. F. Thorpe. Effective-medium theory of percolation on central-force elastic networks. ii. further results. *Physical Review B*, 31(11):7276, 1985.

[75] A. Prasanna Kumart and G. Baskaran. Coherent Potential Approximation, averaged T-matrix approximation and Lloyd's model. *J.Phys. C: Solid State Phys.*, 6, 1973.

[76] X. Mao and T. C. Lubensky. Coherent potential approximation of random nearly isostatic kagome lattice. *Physical Review E*, 83(1):011111, 2011.